
Article:
Ng, C.T. orcid.org/0000-0002-0663-4798 and Susmel, L. orcid.org/0000-0001-7753-9176 (2025) Quantitative review of critical plane criteria and stress analysis approaches for multiaxial fatigue of welded joints. Fatigue & Fracture of Engineering Materials & Structures, 48 (4). pp. 1393-1428. ISSN 8756-758X

https://doi.org/10.1111/ffe.14571

Fatigue & Fracture of Engineering Materials & Structures

WILEY

FFEMS Fatigue & Fracture of Engineering Materials & Structures

INVITED REVIEW OPEN ACCESS

Quantitative Review of Critical Plane Criteria and Stress Analysis Approaches for Multiaxial Fatigue of Welded Joints

Chin Tze Ng[1] | Luca Susmel[2]

[1]School of Mechanical, Aerospace and Civil Engineering, The University of Sheffield, Sheffield, UK | [2]Materials and Engineering Research Institute, Sheffield Hallam University, Sheffield, UK

Correspondence: Luca Susmel (l.susmel@shu.ac.uk)

Received: 28 October 2024 | **Revised:** 16 December 2024 | **Accepted:** 30 December 2024

Keywords: constant amplitude | critical plane | effective notch stress | hot-spot stress | multiaxial fatigue | nominal stress | TCD | variable amplitude | welded joints

ABSTRACT

This quantitative review evaluates the effectiveness of stress-based critical plane criteria, specifically Findley's criterion, the approach due to Carpinteri–Spagnoli (CS), and the Modified Wöhler Curve Method (MWCM), in assessing fatigue strength in aluminum and steel welded joints subjected to constant amplitude (CA) and variable amplitude (VA) multiaxial loading. These criteria were analyzed alongside stress analysis approaches, including nominal stress (NS), hot-spot stress (HSS), effective notch stress (ENS), and the Theory of Critical Distances–Point Method (TCD PM). Results confirm that all criteria effectively estimate fatigue life for steel welded joints under CA loading, with MWCM combined with HSS proving most accurate. For aluminum joints, estimations showed greater conservatism and scatter, highlighting the need for further experimental data to improve accuracy. Experimentally calibrated constants significantly enhanced prediction reliability. Future research should refine these criteria for diverse aluminum grades and thicknesses, ensuring accurate estimations and robust alternatives to established codes.

1 | Introduction

Fatigue in welded joints has been a critical challenge in structural engineering due to several inherent complexities. These include stress concentration at geometric discontinuities, such as notches or sharp corners at weld toes and roots, as well as residual stresses resulting from the rapid thermal cycles during welding. Material inhomogeneity among the filler metal, base material, and heat-affected zone (HAZ) further complicates fatigue behavior. Additionally, surface and internal defects, such as pores or lack of fusion, also increase fatigue susceptibility. When these factors are combined with multiaxial loading under both constant (CA) and variable amplitudes (VA), the risk of fatigue failure in welded joints increases substantially.

To address these challenges, a range of fatigue criteria have been developed to capture the complexities of multiaxial loading and provide accurate fatigue life estimates. These multiaxial fatigue criteria are generally categorized into three main approaches: interaction equation criteria, critical plane criteria, and energy-based criteria.

Interaction equation criteria, commonly recommended by standards like Eurocode 3 (EC3) and the recommendations from the International Institute of Welding (IIW), simplify the multiaxial fatigue problem by modeling the interaction between normalized normal and shear stresses [1–5]. Although practical and easy to use, these methods can struggle with complex stress states, particularly under nonproportional or VA loading [4, 6, 7]. To overcome these limitations, more advanced criteria, including critical plane and energy-based criteria, have been developed. These criteria offer a more accurate representation of fatigue damage, particularly under complex real-world multiaxial loading scenarios.

Summary

- Critical plane criteria with stress analysis validated for multiaxial weld fatigue.
- MWCM with HSS provides the most accurate fatigue life predictions estimations.
- Experimental calibration improves fatigue life accuracy for nonstandard configurations.
- Further research needed for aluminum welds across grades, thicknesses, and load cases.

Critical plane criteria are broadly classified into three variations: strain-based, stress-based, and integral-based approaches. Strain-based criteria, such as those proposed by Smith, Watson, and Topper (SWT), by Brown and Miller, and by Fatemi and Socie, are effective for low-cycle fatigue where plastic deformation plays a crucial role [8–13]. Stress-based criteria, including those proposed by Findley, Matake, McDiarmid, Dang Van, Carpinteri, and Spagnoli, and the so-called Modified Wöhler Curve Method (MWCM) are suited for medium to high-cycle fatigue [14–23]. These criteria describe the linear relationship between stress amplitudes or range and fatigue life, typically represented by an *S–N* curve, and are especially useful for ductile materials like steel, where shear stress (Mode II) governs failure. In contrast, for brittle materials like cast iron, where failure is driven by normal stress (Mode I), criteria based on normal or maximum principal stress are more suitable [24, 25]. Integral-based approaches, like the effective equivalent stress hypothesis (EESH) by Sonsino, focus on fatigue damage accumulation by integrating shear stresses across multiple critical planes, making them suitable for ductile materials such as steel welded joints [26, 27].

Energy-based criteria, on the other hand, assume that the elastic and plastic energy dissipated at crack initiation sites accurately represents fatigue damage. These approaches estimate fatigue life by assessing strain energy density in critical regions [28–33].

Despite extensive research on multiaxial fatigue criteria, existing studies often either focus on a single criterion across different stress analysis methods (e.g., nominal stress [NS], hot-spot stress [HSS], and effective notch stress [ENS]) or evaluate multiple multiaxial fatigue criteria using only one stress analysis approach [4, 5, 34–41]. This fragmented approach limits a comprehensive understanding of how stress-based critical plane criteria perform across various stress analysis methods. This paper addresses this gap by integrating multiple stress-based critical plane criteria for steel and aluminum welded joints under both CA and VA multiaxial fatigue loading. Specifically, it provides a quantitative review of three stress-based critical plane criteria, namely, Findley's criterion, the CS criterion, and the MWCM. By evaluating these criteria through various stress analysis methods, the paper aims to enhance the understanding of fatigue behavior in welded joints and improve the accuracy of fatigue life estimations for practical engineering applications.

2 | Fundamentals of Stress-Based Critical Plane Criteria

Findley's criterion determines the most critical plane based on combined shear and normal stresses. The fatigue damage parameter, f, is derived from the shear stress amplitude, $\Delta\tau/2$, and the maximum normal stress, σ_{max}, with a material constant, β, that indicates sensitivity to normal stress [14, 15, 35, 42]. For ductile materials like steel and aluminum, it was found that β is typically 0.3, and this value will be applied in our analysis of welded joints [4, 14, 15, 43].

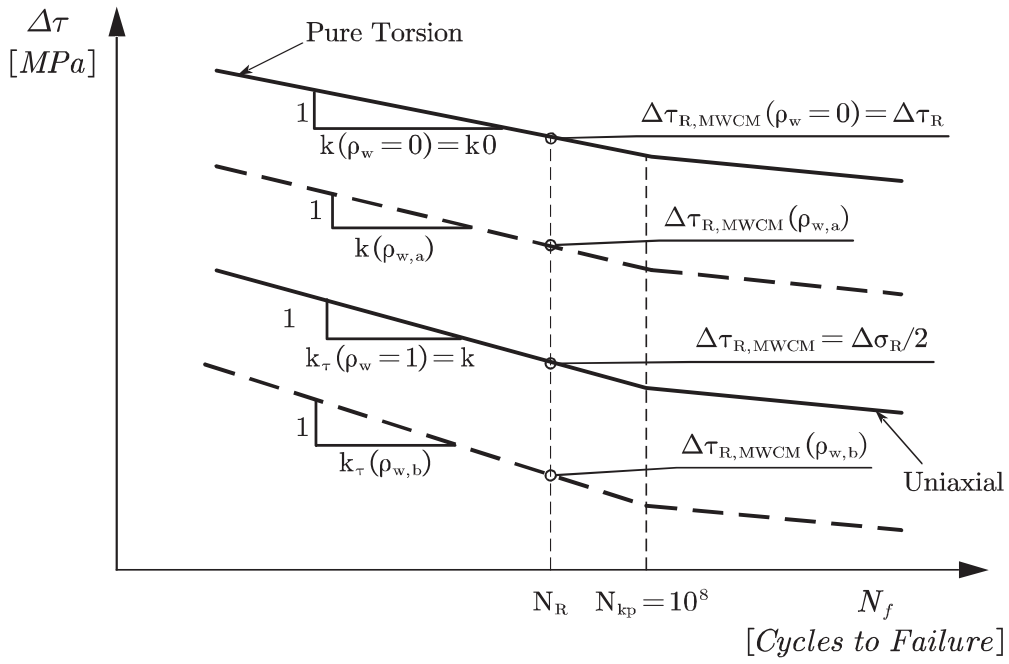

FIGURE 1 | Modified Wöhler diagram illustrating the variation of ρ_w plotted in terms of $\Delta\tau$.

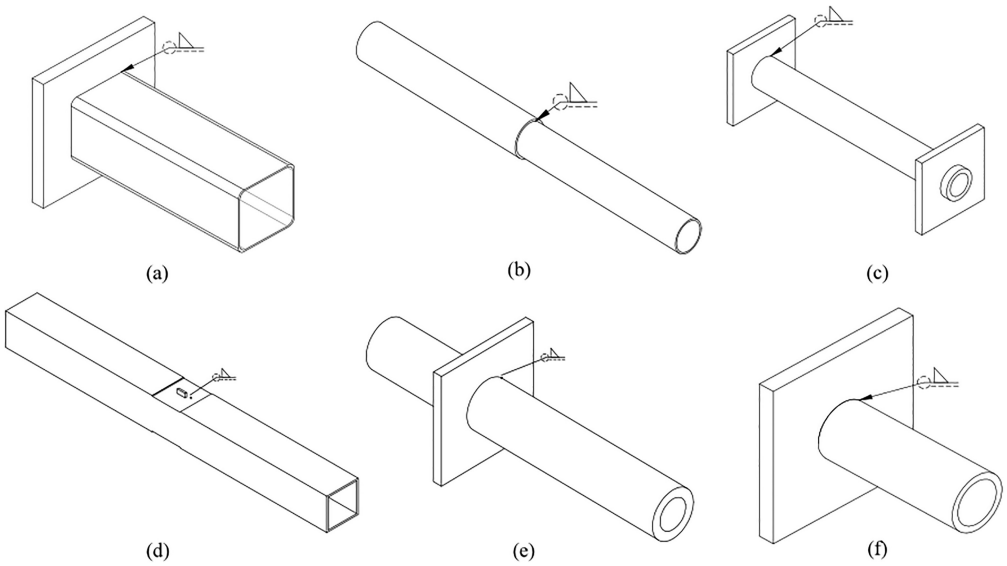

FIGURE 2 | Geometrical configurations of the investigated welded joints.

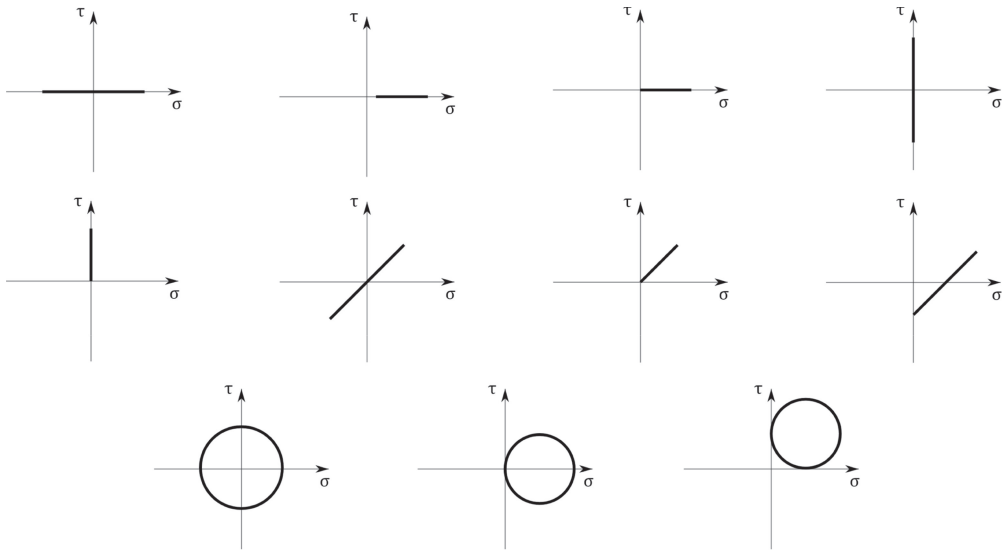

(a)

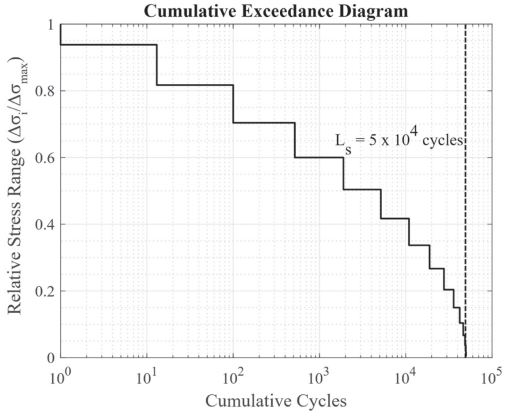

(b)

FIGURE 3 | Fatigue loading paths for CA (a) and LBF Gaussian loading spectrum for VA (b).

TABLE 1 | Summary of reanalyzed welded joints using *NS approach* combined with critical plane criteria under *CA* and *VA* loading, detailing uniaxial and torsional reference fatigue strengths, joint geometries, materials, fatigue curve slopes, and data sources.

	Uniaxial curve slope, k						Torsional curve slope, k_0							
	$\Delta\sigma_{R,Ps=97.7\%}$ [a] (MPa)		k (before knee point)[b]		k^* (after knee point)[b]		$\Delta\tau_{R,Ps=97.7\%}$ [a] (MPa)		k_0 (before knee point)[c]		$k_0{}^*$ (after knee point)[c]			
Material (CA)	**IIW**	**Exp**[d]	**IIW**	**Exp**[d]	**IIW**	**Exp**[d]	**IIW**	**Exp**[d]	**IIW**	**Exp**[d]	**IIW**[e]	**Exp**[d]	**Geometry**	**Reference**
UM StE 460[f]	71	142.7	3	4.4	22	22	100	127.5	5	4.9	22	22	Figure 4f	[26]
M StE 460[f]	71	166.5	3	4.6	22	22	100	—	5	—	22	22	Figure 4f	[73]
UM StE 460[f]	71	194.7	3	4.2	22	22	100	—	5	—	22	22	Figure 4b	[73]
M StE 460[f]	71	321.6	3	8.2	22	22	100	128.0	5	6.3	22	22	Figure 4b	[73]
StE 460[f]	71	116.4	3	4.2	22	22	100	180.9	5	7.3	22	22	Figure 4f	[79]
StE 460	71	122.9	3	5.4	22	22	100	80.5	5	6.1	22	22	Figure 4f	[67]
A519	71	96.3	3	5.4	22	22	80	94.2	5	3.7	22	22	Figure 4e	[78]
A519-A36[f]	80	144.4	3	3.8	22	22	100	104.2	5	5.5	22	22	Figure 4d	[77]
BS4360 Gr.50E	71	65.6	3	3.0	22	22	80	66.3	5	4.5	22	22	Figure 4c	[71]
Fe 52 steel	45	15.8	3	2.3	22	22	100	44.1	5	3.5	22	22	Figure 4a	[66]
BS4360	80	—	3	—	22	22	80	—	5	—	22	22	Figure 4d	[65]
S340 + N, E355 + N	71	204.2	3	6.1	22	22	100	207.8	5	6.6	22	22	Figure 4b	[72]
S340 + N, E355 + N[f]	71	44.6	3	2.9	22	22	100	71.3	5	3.6	22	22	Figure 4b	[72]
St 35 ($t = 1$ mm)	71	69.2	3	4.9	22	22	100	106.4	5	8.4	22	22	Figure 4b	[70]
St 35 ($t = 2$ mm)	71	66.4	3	5.3	22	22	100	74.5	5	6.1	22	22	Figure 4b	[76]
6082-T6	32	55.0	3	6.9	22	22	36	50.4	5	6.2	22	22	Figure 4f	[74]
6060-T6[f]	22	84.1	3	5.5	22	22	36	—	5	—	22	22	Figure 4b	[68]
AW 6082	22	20.3	3	4.2	22	22	36	42.3	5	5.8	22	22	Figure 4b	[70]
AW 5042	22	16.6	3	4.1	22	22	36	42.5	5	5.9	22	22	Figure 4b	[70]

TABLE 1 | (Continued)

Material (VA)	$\Delta\sigma_{R,Ps=97.7\%}$ [a] (MPa)		Uniaxial curve slope, k				$\Delta\tau_{R,Ps=97.7\%}$ [a] (MPa)		Torsional curve slope, k_0				Geometry	Reference
			k (before knee point) [b]		k' (after knee point) [b]				k_0 (before knee point) [c]		k_0' (after knee point) [c]			
	IIW	Exp [d]	IIW	Exp [d]	IIW [e]	Exp [d]	IIW	Exp [d]	IIW	Exp [d]	IIW [e]	Exp [d]		
StE 460 [f]	71	142.7	3	4.4	5	7.8	100	127.5	5	4.9	9	8.8	Figure 4f	[27]
StE 460 [f]	71	116.4	3	3.9	5	6.8	100	180.9	5	7.3	9	13.6	Figure 4f	[79]
42CrMo4 [f]	—	—	—	—	—	—	100	—	5	—	9	—	Figure 4b	[80]
6082-T6	32	55.0	3	6.9	5	12.8	36	42.3	5	6.3	9	11.6	Figure 4f	[75]

Abbreviations: M—machined; UM—unmachined.
[a]Reference normal and shear stresses extrapolated at two million cycles to failure, with $P_s = 97.7\%$.
[b]The knee point for the IIW in terms of normal stress corresponds to $N_{kp} = 10^7$ cycles.
[c]The knee point for the IIW in terms of shear stress corresponds to $N_{kp} = 10^8$ cycles.
[d]Exp refers to experimental data.
[e]Slopes (k' and k_0') suggested by the IIW for VA loading are derived from Haibach's modification ($2k-1$), where k is the slope before the knee point.
[f]Stress relieved.

The original formulation of Findley's criterion is expressed as

$$f = \left(\frac{\Delta\tau}{2} + \beta\sigma_{\max}\right). \tag{1}$$

The critical plane is identified where this combined effect is maximized. To simplify multiaxial fatigue assessment, Bruun and Härkegård proposed a reformulation into an equivalent uniaxial stress range [4, 15]:

$$\Delta\sigma_{\text{find}} = \frac{\Delta\tau + 2\beta\sigma_{\max}}{\frac{1}{2}\left(\beta + \sqrt{1+\beta^2}\right)} \le \Delta\sigma_R. \tag{2}$$

This reformulated version will be employed to evaluate Findley's criterion in conjunction with various stress analysis approaches.

The CS criterion employs a critical plane approach to assess multiaxial fatigue by correlating the orientation of the critical plane with the principal stress directions. It assumes that the critical plane coincides with the weighted mean direction of the principal stresses when the first principal normal stress reaches its peak during a fatigue cycle [20–22, 44, 45]. The CS damage parameter is expressed as a nonlinear function combining the ranges of normal and shear stresses acting on this critical plane, modified by the squared ratio of their respective reference fatigue strengths in normal, $\Delta\sigma^2_{R=-1}$, and shear, $\Delta\tau^2_{R=-1}$, under fully reversed loading conditions ($R=-1$). Additionally, the CS criterion incorporates a Goodman correction to account for mean stress effects. The mathematical formulation of the CS criterion is provided in Equations (3) and (4) [20–22, 44, 45]:

$$\Delta\sigma_{CS} = \sqrt{\Delta\sigma^2_{eq} + \left(\frac{\Delta\sigma^2_{R=-1}}{\Delta\tau^2_{R=-1}}\right)\cdot\Delta\tau^2}, \tag{3}$$

$$\Delta\sigma_{eq} = \Delta\sigma + \Delta\sigma_{R=-1}\left(\frac{\sigma_m}{\sigma_u}\right), \tag{4}$$

where σ_m is the mean normal stress and σ_u is the ultimate tensile strength of the material. The off angle, δ, between the normal to the critical plane and the average direction of the first principal stress, is computed using the empirical equation shown in Equation (5) [20–22, 44, 45]:

$$\delta = \begin{cases} \frac{3\pi}{8}\left[1-\left(\frac{\Delta\tau_{R=-1}}{\Delta\sigma_{R=-1}}\right)^2\right], & \text{if } \frac{1}{\sqrt{3}} \le \frac{\Delta\tau_{R=-1}}{\Delta\sigma_{R=-1}} \le 1, \\ \frac{\pi}{4}, & \text{if } \frac{\Delta\tau_{R=-1}}{\Delta\sigma_{R=-1}} < \frac{1}{\sqrt{3}}, \\ 0, & \text{if } \frac{\Delta\tau_{R=-1}}{\Delta\sigma_{R=-1}} > 1. \end{cases} \tag{5}$$

It is important to highlight that the reference fatigue strengths for fully reversed uniaxial and pure torsional loading are not

directly applicable to standard reference curves, such as those recommended by the IIW. These IIW curves were generated for higher R ratios to account for worst-case as-welded conditions. Therefore, in this reanalysis, the IIW-recommended reference fatigue strength is substituted in Equation (3). However, for experimentally derived reference curves, the original fully reversed uniaxial, $\Delta\sigma_{R=-1}$, and pure torsional, $\Delta\tau_{R=-1}$, fatigue strengths will be applied as outlined in the original, rigorous formulation of the CS criterion.

The MWCM is a biparametric critical plane approach that focuses on shear stress. It identifies the critical plane as the one experiencing both the maximum shear stress range and the maximum normal stress range, simultaneously [23, 37–39, 46–49]. To assess the complexity of multiaxial fatigue in welded joints, the MWCM introduces a stress ratio, ρ_w, defined in Equation (6), which characterizes the degree of multiaxiality at the critical plane. Specifically, $\rho_w = 1$ under uniaxial conditions and $\rho_w = 0$ under pure torsional loading.

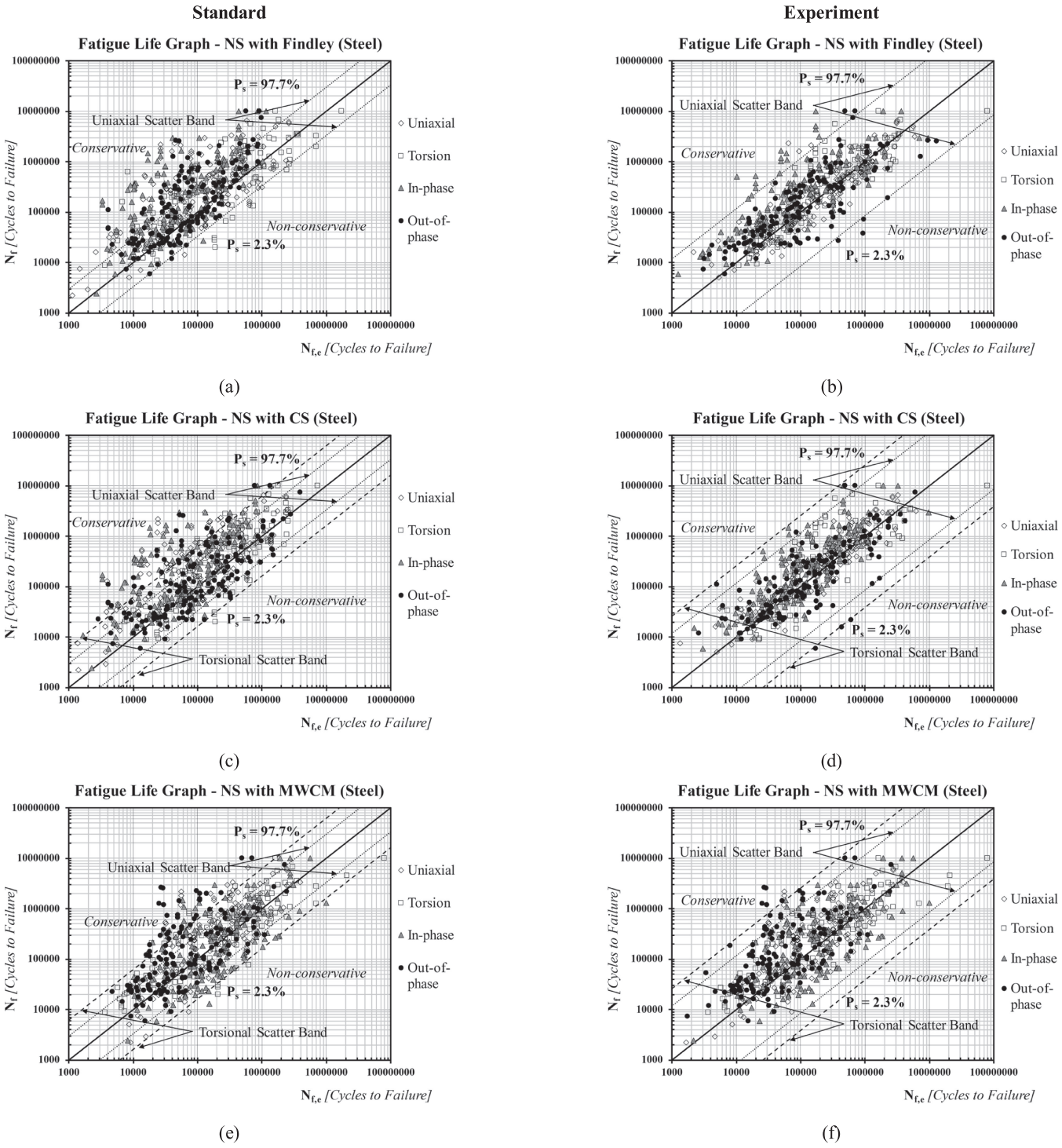

FIGURE 4 | Nominal stress (NS) approach: Fatigue life graphs for as-welded and stress-relieved *steel* welded joints using Findley's criterion (a,b), the CS approach (c,d), and the MWCM (e,f) under *CA* fatigue loading, comparing standard and experimental reference strength based on $P_s = 50\%$.

$$\rho_w = \frac{\Delta\sigma_n}{\Delta\tau}. \quad (6)$$

The MWCM is visually represented through a modified Wöhler diagram, which plots $\Delta\tau$ against the number of cycles to failure, N_f, as shown in Figure 1 [23, 37–39, 46–49].

From this diagram, key parameters such as the negative inverse slope, k_τ, and the reference stress range, $\Delta\tau_{R,MWCM}$, are represented as linear functions. These functions are calibrated using both uniaxial and pure torsional reference curves. The calibration formulas for k_τ and $\Delta\tau_{R,MWCM}$ are given in Equations (7) and (8):

$$k_\tau(\rho_w) = \left[k_\tau(\rho_w = 1) - k_\tau(\rho_w = 0)\right]\rho_w + k_\tau(\rho_w = 0), \quad (7)$$

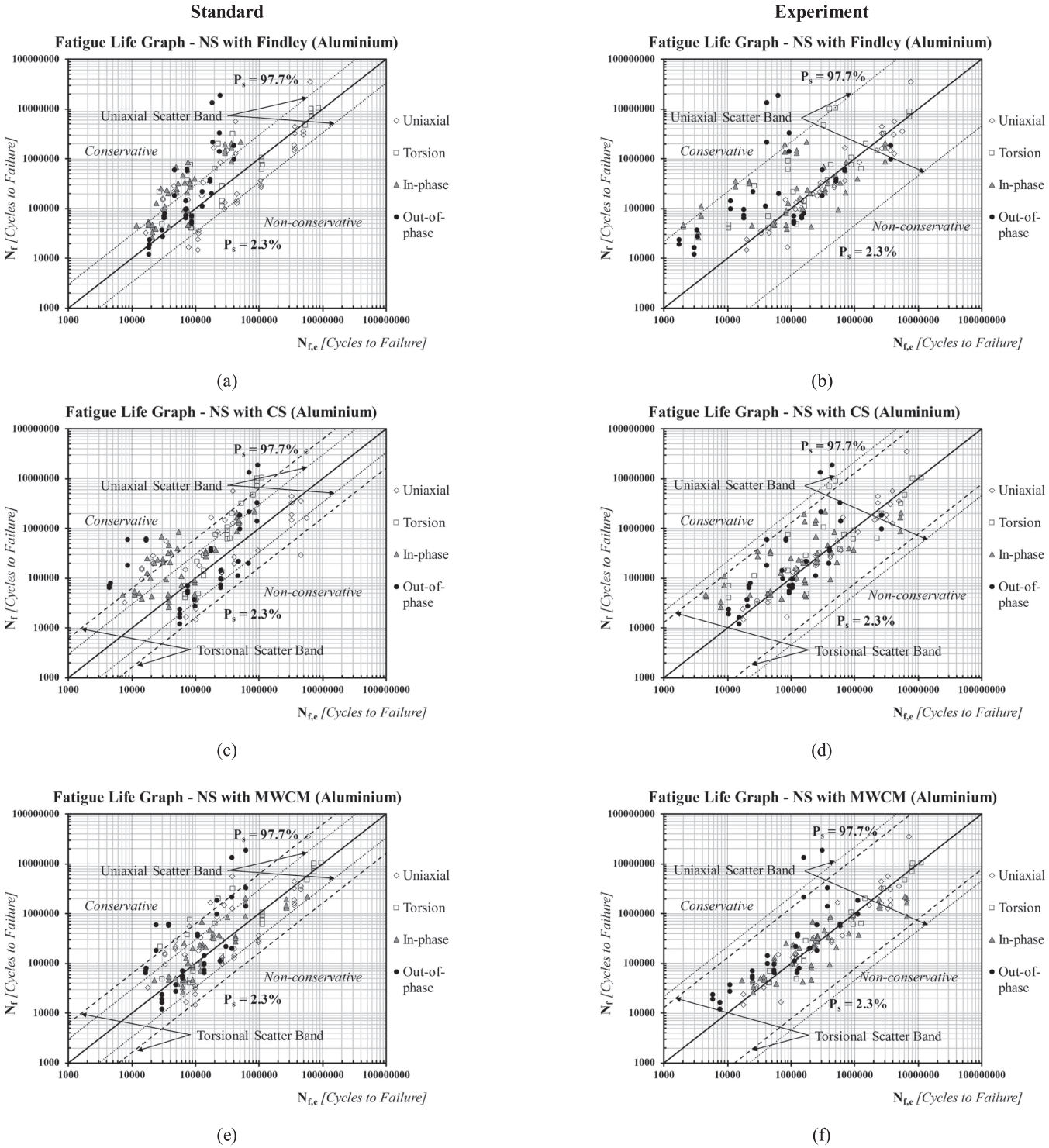

FIGURE 5 | Nominal stress (NS) approach: Fatigue life graphs for as-welded and stress-relieved *aluminum* welded joints using Findley's criterion (a,b), the CS approach (c,d), and the MWCM (e,f) under *CA* fatigue loading, comparing standard and experimental reference strength based on $P_s = 50\%$.

$$\Delta\tau_{R,MWCM}(\rho_w) = \left(\frac{\Delta\sigma_R}{2} - \Delta\tau_R\right)\rho_w + \Delta\tau_R. \quad (8)$$

To avoid excessive conservatism at high values of ρ_w, a threshold limit $\rho_{w,lim}$ is applied, as outlined in Equation (9) [23, 37].

$$\rho_{w,lim} = \frac{\Delta\tau_R}{2\Delta\tau_R - \Delta\sigma_R}, \quad (9)$$

This limit is based on experimental evidence showing that overly conservative results occur at high ρ_w values. The introduction of this limit ensures a more accurate assessment of fatigue damage on the critical plane.

Under CA loading, applying multiaxial fatigue criteria is relatively simple, as closed cycles can be easily identified. However, under VA loading conditions, defining a closed cycle becomes more challenging, necessitating the use of cycle

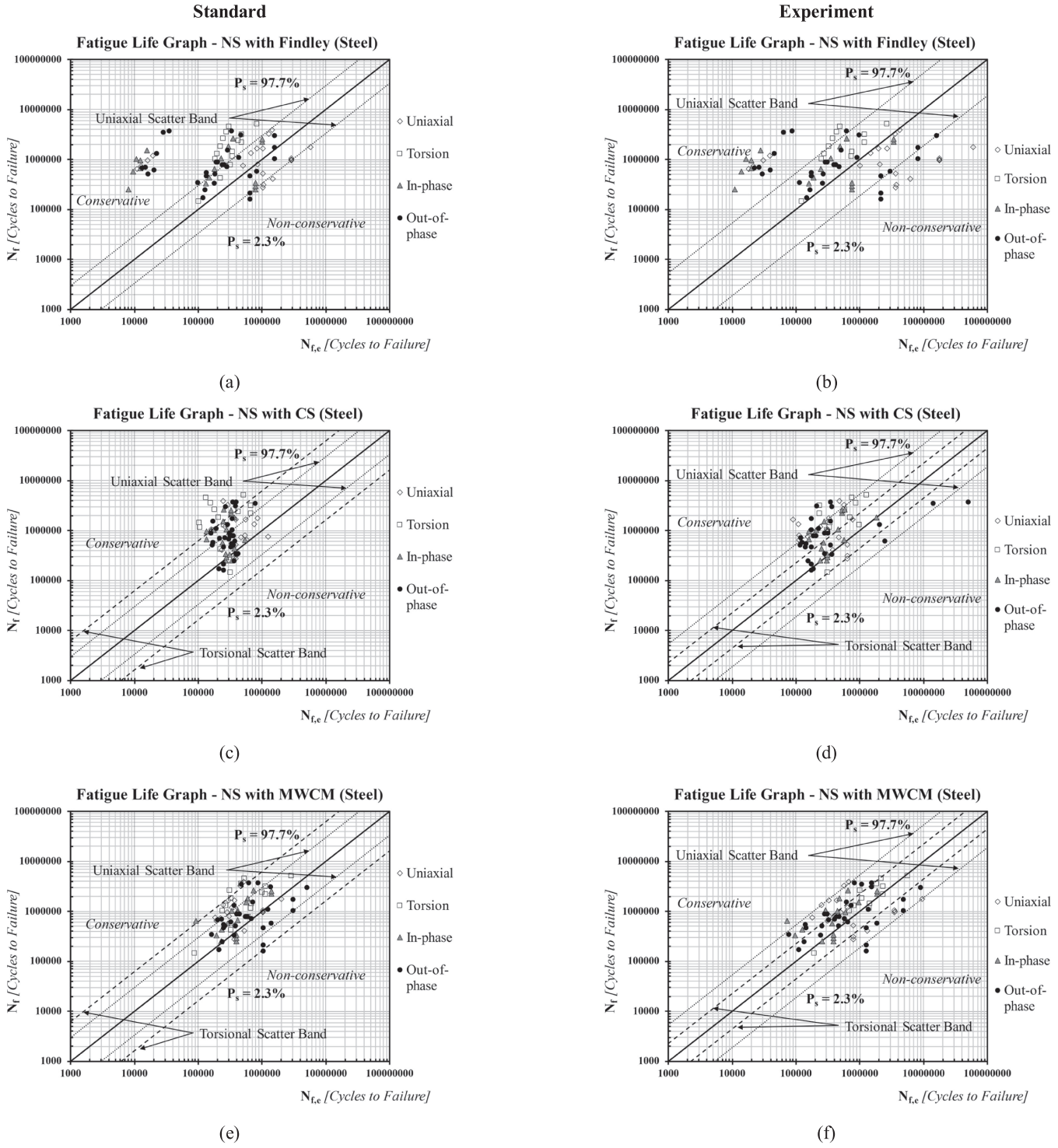

FIGURE 6 | Nominal stress (NS) approach: Fatigue life graphs for as-welded and stress-relieved *steel* welded joints using Findley's criterion (a,b), the CS approach (c,d), and the MWCM (e,f) under *VA* fatigue loading, comparing standard and experimental reference strength based on $P_s = 50\%$.

counting techniques [50–54]. One of the most widely adopted methods is the rainfall counting method, originally introduced by Matsuishi using the "pagoda roof" concept [54, 55]. Over time, variations such as the three-point and four-point rainflow methods have been developed, with the ASTM version gaining popularity due to its computational efficiency [50–54, 56].

The conventional rainflow method is particularly effective for fatigue assessments involving a single loading component, such as those governed by the Gough–Pollard criterion or the EC3 interaction equation [1, 57]. However, when both normal and shear stress cycles need to be considered simultaneously, the conventional rainflow method struggles to define closed cycles in multiaxial loading scenarios [35].

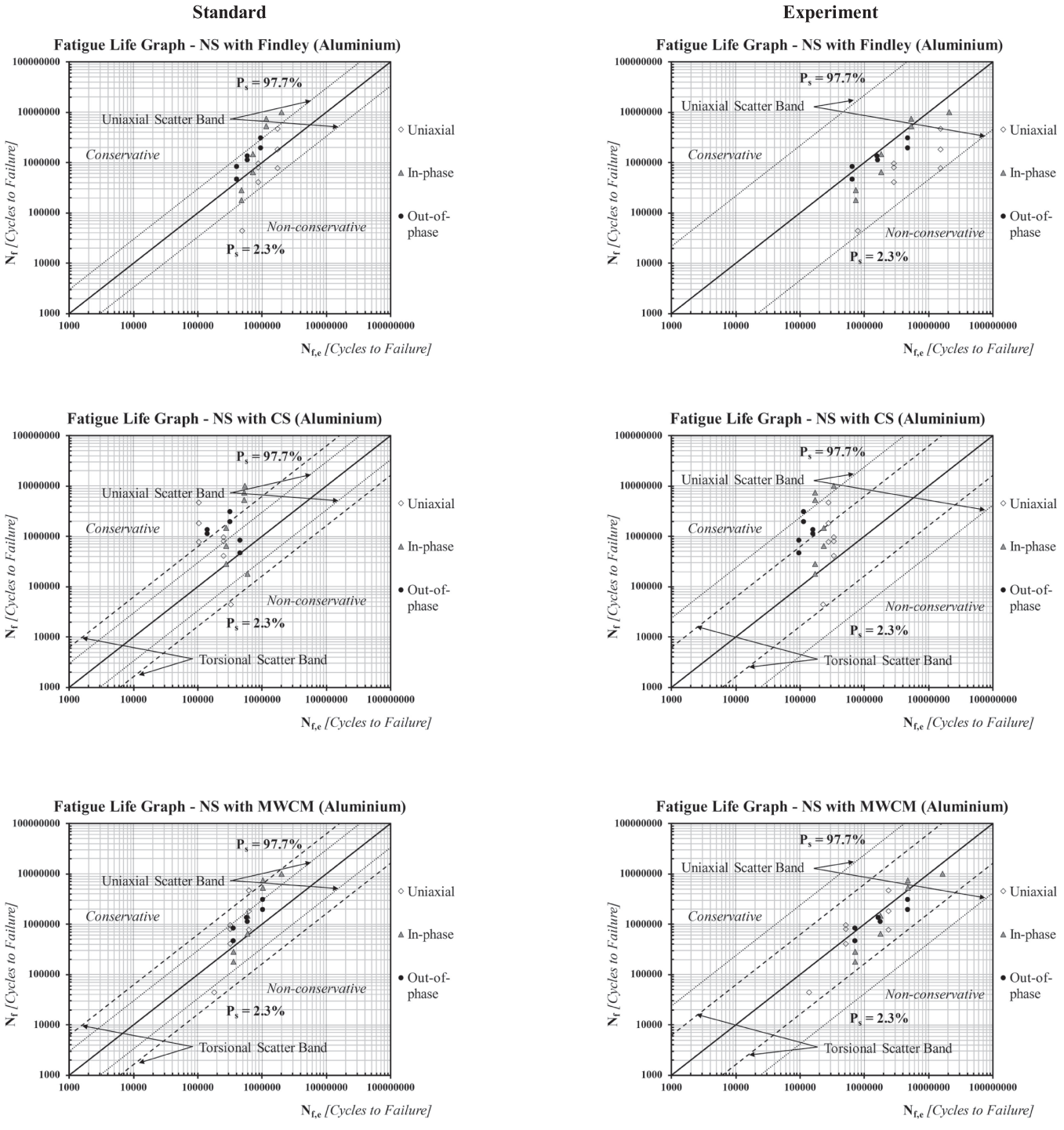

FIGURE 7 | Nominal stress (NS) approach: Fatigue life graph for as-welded and stress-relieved *aluminum* welded joints using Findley's criterion (a,b), the CS approach (c,d), and the MWCM (e,f) under *VA* fatigue loading, comparing standard and experimental reference strength based on $P_s = 50\%$.

To overcome this limitation, Carpinteri et al. proposed the CS counting method, capable of simultaneously evaluating normal and shear stress cycles [21]. This approach simplifies the process by first identifying closed cycles in the normal stress time signal, which, as a scalar function, makes cycle identification more straightforward. Once the normal stress cycles are identified, the corresponding shear stress range is computed using methods like the longest chord or minimum circumscribed circle within the defined normal stress cycles [58]. Detailed explanations of the CS counting method can be found in the original reference [21].

By focusing first on normal stress cycles and then incorporating shear stress, the CS counting method effectively handles multiaxial fatigue criteria that require both components, such as Findley's criterion and the CS criterion [21, 35, 56]. This paper adopts the CS counting method to reassess the fatigue damage in welded joints under VA loading for a more accurate evaluation.

In contrast, the MWCM being a shear stress-based multiaxial fatigue criterion takes a different approach to handling VA loading. Susmel's maximum variance method (MVM) simplifies the multiaxial stress problem by identifying the plane with the maximum shear stress variance, which is then used as the critical stress range. Equations (10–12) provide the mathematical formulations for the effective shear stress range, variance, and mean value relative to the critical plane [37, 59–61].

$$\Delta\tau_{MWCM} = 2 \cdot \sqrt{2 \cdot Var\left[\tau_{MV}(t)\right]}, \tag{10}$$

$$Var\left[\tau_{MV}(t)\right] = \frac{1}{T}\int_0^T \left[\tau_{MV}(t) - \tau_m\right]^2 \cdot dt, \tag{11}$$

$$\tau_m = \frac{1}{T}\int_0^T \tau_{MV}(t) \cdot dt. \tag{12}$$

By reducing the shear stress to a unidimensional quantity, MVM avoids the complexities of accounting for both normal and shear stress cycles simultaneously. This allows the conventional three-point rainflow cycle counting method, as standardized by ASTM, to be applied because only a single effective shear stress range needs to be considered [37, 51, 59–61].

In this reanalysis, both the CS counting method, combined with Findley's criterion and the CS approach, and MVM, applied with the MWCM, will be used to effectively address VA loading conditions and assess the fatigue damage in welded joints.

3 | Validation Methods for Critical Plane Criteria

The validation of critical plane multiaxial fatigue criteria focuses on analyzing welded joint configurations under both CA and VA fatigue loading conditions. These criteria are assessed in conjunction with various stress analysis approaches, including NS, HSS, ENS, and the Theory of Critical Distances–Point Method (TCD PM) [1–3, 36, 37, 48, 62–64]. As illustrated in Figure 2, the welded joint configurations include both as-welded and stress-relieved joints [26, 27, 65–79]. The investigated welded joints display a broad range of dimensions, with plate thicknesses ranging from 1.5 to 10 mm, weld leg sizes from 0.8 to 11 mm, and overall lengths from 107.5 to 2040 mm. The limitation of plate thickness to 10 mm is solely due to the availability of experimental data in the existing literature on welded joints tested under multiaxial fatigue loading. This extensive range ensures the validation covers a wide array of welded configurations, allowing for a comprehensive and detailed assessment of the multiaxial fatigue criteria.

Additionally, the quantitatively reviewed fatigue data for CA loading includes various loading path conditions, which can be broadly classified into four categories: uniaxial, pure torsional, in-phase, and out-of-phase loading [26, 27, 65–79].

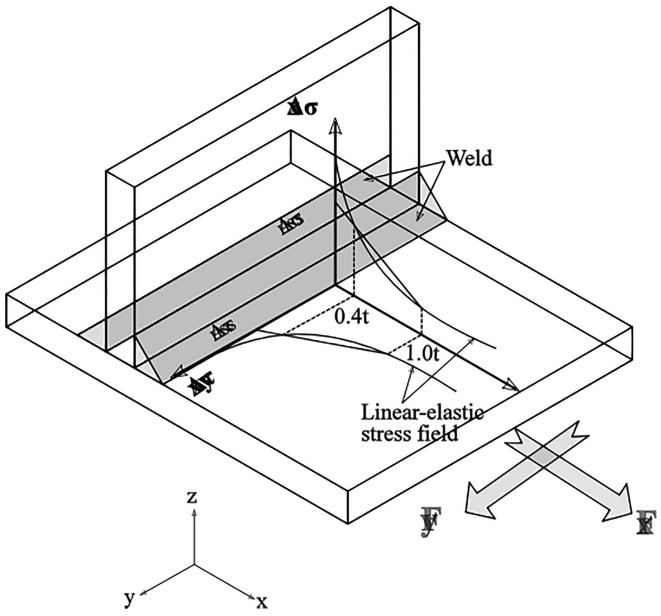

FIGURE 8 | Illustration showcasing the application of modified hot-spot stress (HSS) analysis approach.

TABLE 2 | Summary of reanalyzed welded joints using *HSS approach* combined with critical plane criteria under *CA* and *VA* loading, detailing uniaxial and torsional reference fatigue strengths, joint geometries, materials, fatigue curve slopes, and data sources.

			Uniaxial curve slope, k						Torsional curve slope, k_0					
	$\Delta\sigma_{R,Ps=97.7\%}$[a] (MPa)		k (before knee point)[b]		k^* (after knee point)[b]		$\Delta\tau_{R,Ps=97.7\%}$[a] (MPa)		k_0 (before knee point)[c]		$k_0{}^*$ (after knee point)[c]			
Material (CA)	**IIW**	**Exp[d]**	**IIW**	**Exp[d]**	**IIW**	**Exp[d]**	**IIW**	**Exp[d]**	**IIW**	**Exp[d]**	**IIW**	**Exp[d]**	**Geometry**	**Reference**
UM StE 460[f]	90	188.7	3	4.4	22	22	100	138.7	5	4.9	22	22	Figure 4f	[26]
M StE 460[f]	90	210.0	3	4.6	22	22	100	—	5	—	22	22	Figure 4f	[73]
UM StE 460[f]	90	208.4	3	4.2	22	22	100	—	5	—	22	22	Figure 4b	[73]
StE 460[f]	90	163.1	3	4.2	22	22	100	206.7	5	7.3	22	22	Figure 4f	[79]
A519	90	112.7	3	5.4	22	22	100	100.7	5	3.7	22	22	Figure 4e	[78]
A519-A36[f]	90	153.6	3	3.8	22	22	100	110.7	5	5.5	22	22	Figure 4d	[77]
BS4360 Gr.50E	90	111.7	3	3.0	22	22	80	72.7	5	4.5	22	22	Figure 4c	[71]
Fe 52 steel	90	22.7	3	2.3	22	22	100	48.4	5	3.5	22	22	Figure 4a	[66]
S340 + N, E355 + N	90	343.0	3	6.1	22	22	80	229.2	5	6.6	22	22	Figure 4f	[72]
S340 + N, E355 + N[f]	90	74.8	3	2.9	22	22	100	74.8	5	3.6	22	22	Figure 4f	[72]
6082-T6	36	76.1	3	6.9	22	22	80	55.0	5	6.3	22	22	Figure 4f	[74]
6060-T6[f]	36	122.5	3	5.5	22	22	100	—	5	—	22	22	Figure 4b	[68]

			Uniaxial curve slope, k						Torsional curve slope, k_0					
	$\Delta\sigma_{R,Ps=97.7\%}$[a] (MPa)		k (before knee point)[b]		k' (after knee point)[b]		$\Delta\tau_{R,Ps=97.7\%}$[a] (MPa)		k_0 (before knee point)[c]		$k_0{}'$ (after knee point)[c]			
Material (VA)	**IIW**	**Exp[d]**	**IIW**	**Exp[d]**	**IIW[e]**	**Exp[d]**	**IIW**	**Exp[d]**	**IIW**	**Exp[d]**	**IIW[e]**	**Exp[d]**	**Geometry**	**Reference**
StE 460[f]	71	142.7	3	4.4	5	7.8	100	138.7	5	4.9	9	8.8	Figure 4f	[27]
StE 460[f]	71	116.4	3	3.9	5	6.8	100	206.7	5	7.3	9	13.6	Figure 4f	[79]
42CrMo4[f]	—	—	—	—	—	—	100	—	5	—	9	—	Figure 4b	[80]
6082-T6	32	55.0	3	6.9	5	12.8	36	55.0	5	6.3	9	11.6	Figure 4f	[75]

Abbreviations: M—machined; UM—unmachined.
[a]Reference normal and shear stresses extrapolated at two million cycles to failure, with $P_s = 97.7\%$.
[b]The knee point for the IIW in terms of normal stress corresponds to $N_{kp} = 10^7$ cycles.
[c]The knee point for the IIW in terms of shear stress corresponds to $N_{kp} = 10^8$ cycles.
[d]Exp refers to experimental data.
[e]Slopes (k' and k_0') suggested by the IIW for VA loading are derived from Haibach's modification ($2k - 1$), where k is the slope before the knee point.
[f]Stress relieved.

These categories are assessed across different stress ratios ($R = \sigma_{min}/\sigma_{max}$ or $R = \tau_{min}/\tau_{max}$), such as $R = -1$ and $R = 0$. These loading paths are illustrated in Figure 3a, drawn from reanalyzed CA fatigue tests. For VA fatigue loading, the validation employs a Gaussian load spectrum with a sequence length of 5×10^4 cycles, as depicted in Figure 3b [27, 75, 79, 80]. This spectrum is applied to all reanalyzed welded joints subjected to VA loading conditions.

The validation also accounts for the distinct fatigue behaviors of as-welded and stress-relieved joints. As-welded joints typically retain high residual tensile stresses localized near the

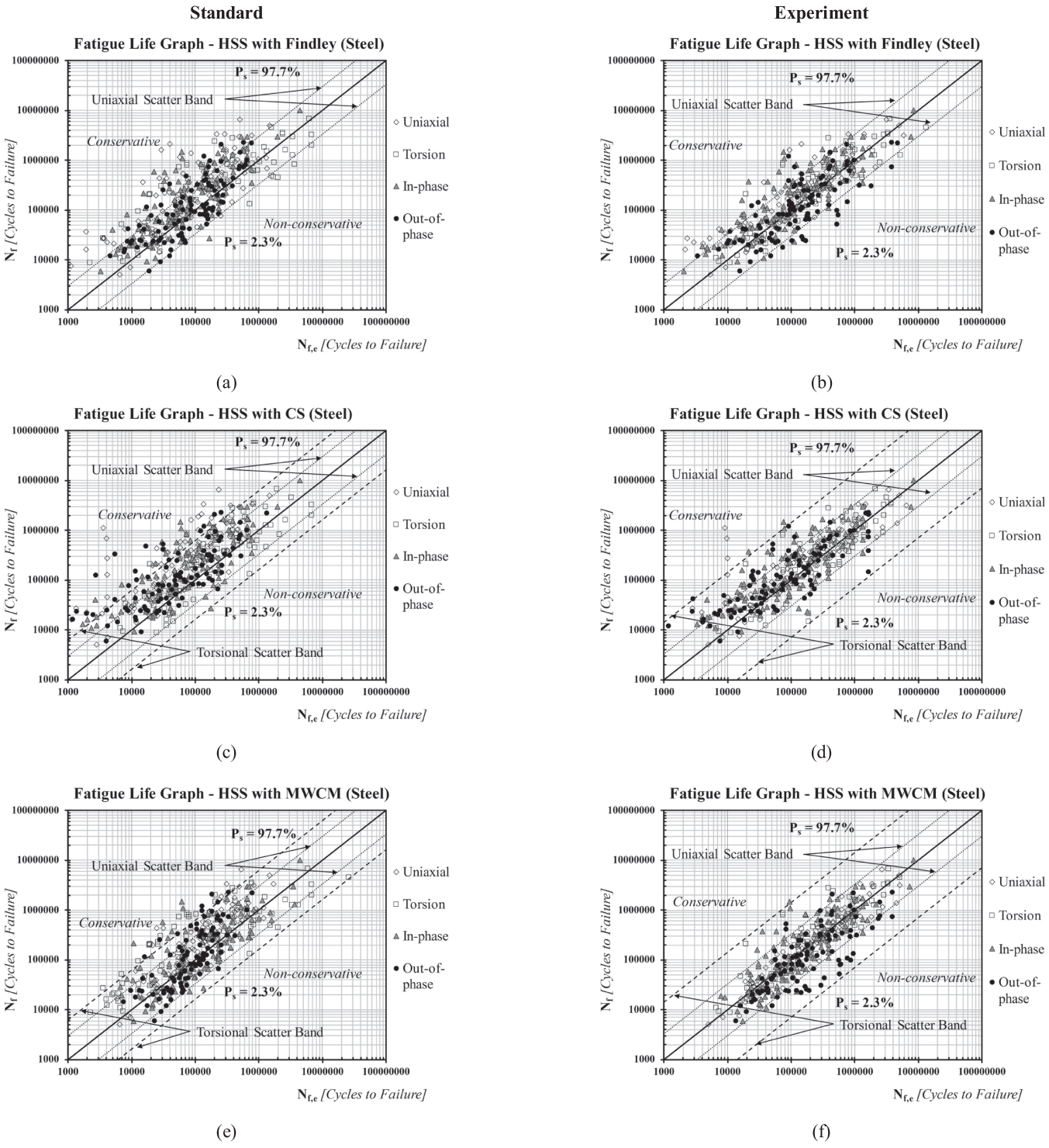

FIGURE 9 | Hot-spot stress (HSS) approach: Fatigue life graphs for as-welded and stress-relieved *steel* welded joints using Findley's criterion (a,b), the CS approach (c,d), and the MWCM (e,f) under *CA* fatigue loading, comparing standard and experimental reference strength based on $P_s = 50\%$.

vicinity of the fatigue crack initiation zone due to the welding process. These residual stresses elevate the local stress ratio even when the global stress ratio is set to $R = -1$ [81, 82]. This increased local stress ratio reduces the influence of mean stress effects, allowing it to be considered negligible in fatigue assessments for as-welded joints [23, 81, 82]. In contrast, stress-relieved joints, having undergone heat treatment to reduce residual stresses, exhibit improved fatigue strength.

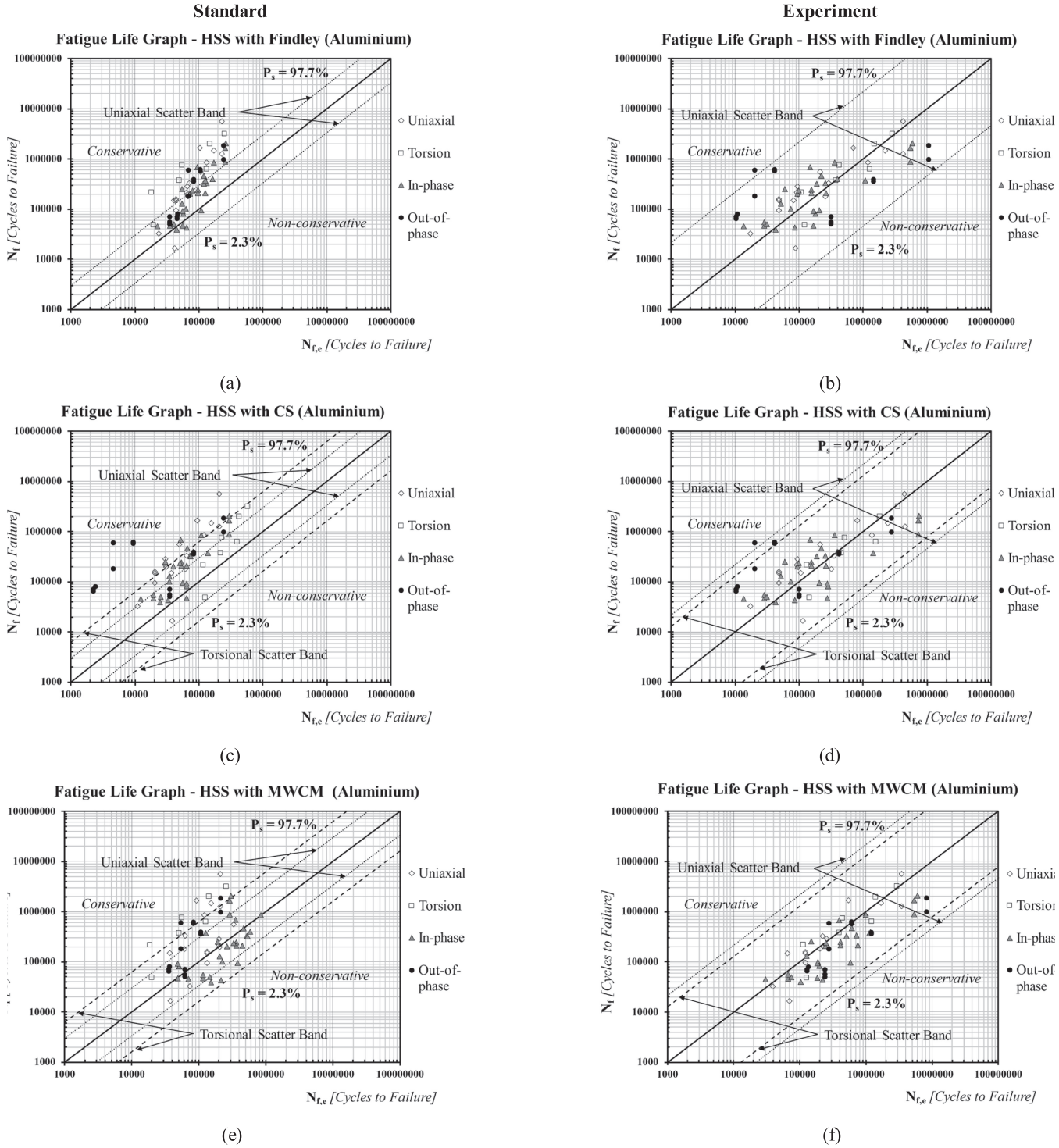

FIGURE 10 | Hot-spot stress (HSS) approach: Fatigue life graphs for as-welded and stress-relieved *aluminum* welded joints using Findley's criterion (a,b), the CS approach (c,d), and the MWCM (e, f) under *CA* fatigue loading, comparing standard and experimental reference strength based on $P_s = 50\%$.

To account for this improvement, enhancement factors are applied according to the FKM guidelines and Sonsino's rules [83–85]. For stress-relieved steel joints, these factors are determined using Equation (13), while for aluminum joints, Equation (14) is used [37, 83–85].

$$\begin{aligned} f(R) &= 1.32; \quad if\, R \le -1, \\ f(R) &= -0.22 \times R + 1.1; \quad if -1 \le R \le 0, \\ f(R) &= -0.2 \times R + 1.1; if\, 0 < R \le 0.5, \\ f(R) &= 1; if\, R > 0.5, \end{aligned} \tag{13}$$

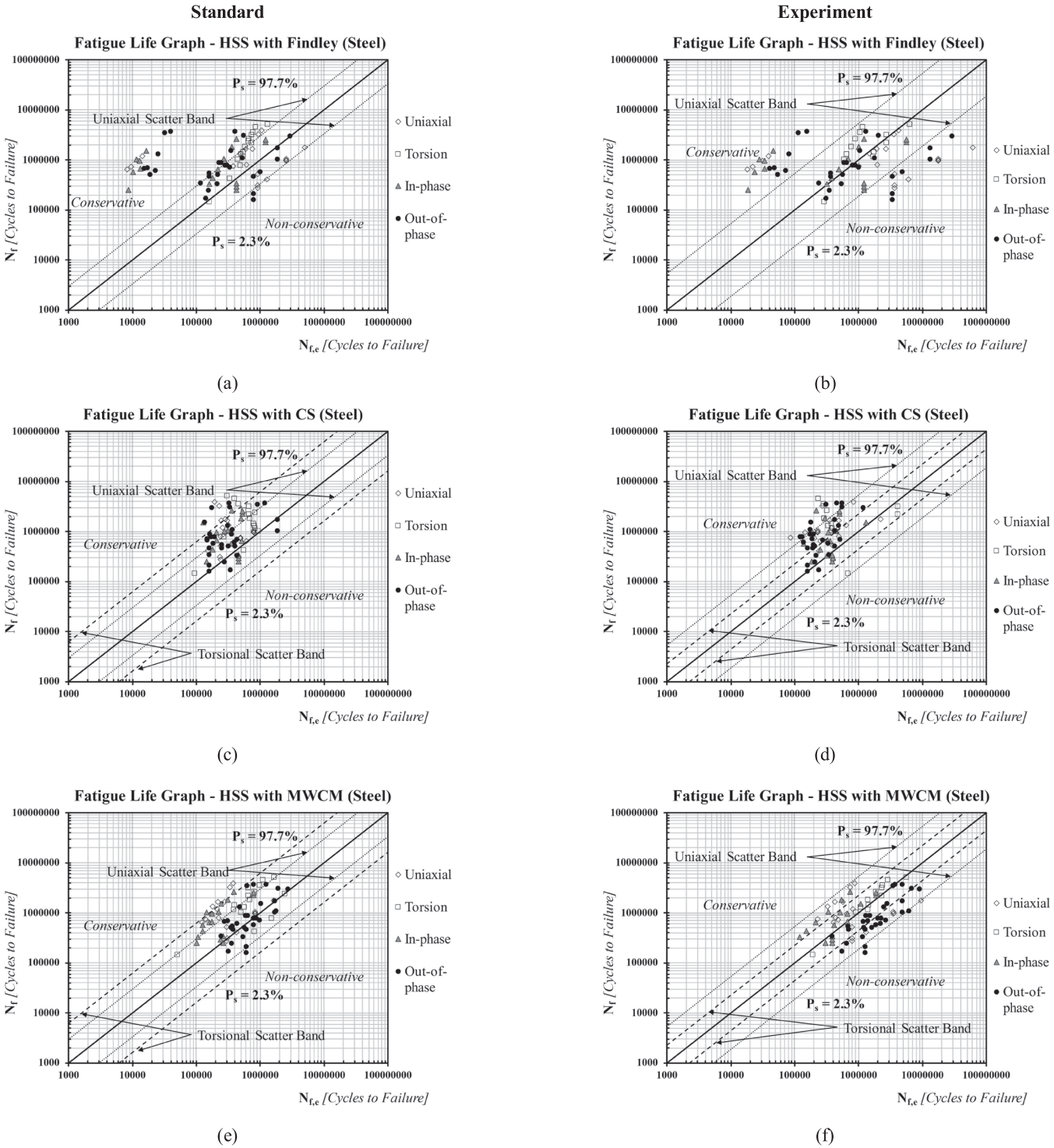

FIGURE 11 | Hot-spot stress (HSS) approach: Fatigue life graph for as-welded and stress-relieved *steel* welded joints using Findley's criterion (a,b), the CS approach (c,d), and the MWCM (e,f) under *VA* fatigue loading, comparing standard and experimental reference strength based on $P_s = 50\%$.

$$
\begin{aligned}
f(R) &= 1.88; \quad if\, R \le -1, \\
f(R) &= -0.55 \times R + 1.33; \quad if -1 \le R \le 0, \\
f(R) &= -0.66 \times R + 1.33; if\, 0 < R \le 0.5, \\
f(R) &= 1; if\, R > 0.5.
\end{aligned} \tag{14}
$$

These adjustments ensure more precise fatigue life estimates, preventing overly conservative estimates across varying loading ratios and materials. However, when assessing the MWCM with the TCD PM, the factors from Equations (13) and (14) are replaced by a simplified rule based on ECs. This rule limits the effective shear stress range by considering only 60% of

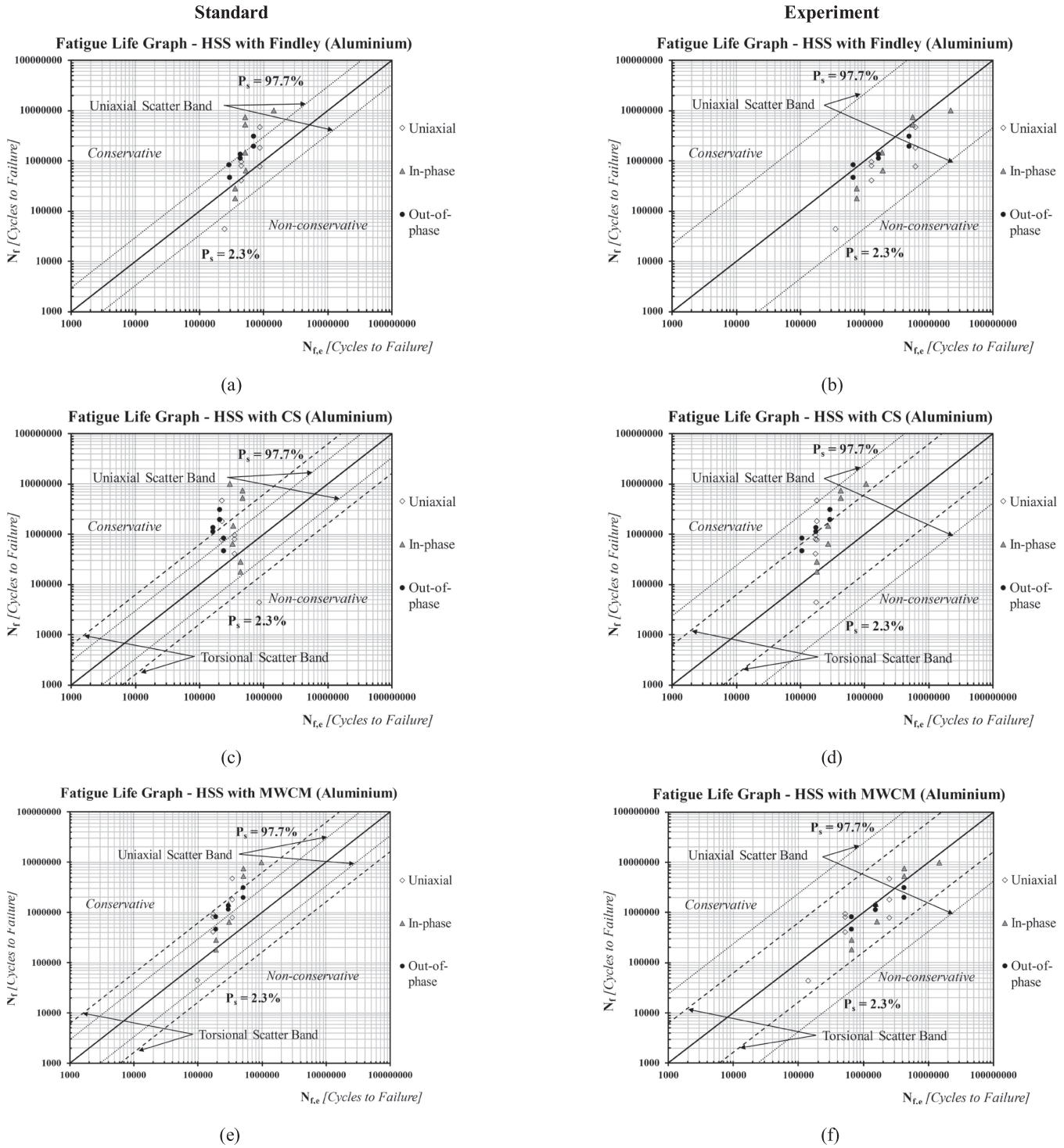

FIGURE 12 | Hot-spot stress (HSS) approach: Fatigue life graph for as-welded and stress-relieved *aluminum* welded joints using Findley's criterion (a,b), the CS approach (c,d), and the MWCM (e,f) under *VA* fatigue loading, comparing standard and experimental reference strength based on $P_s = 50\%$.

the compressive stress range, as specified in EC3 and EC9 [23, 37, 39].

For this validation, two sets of reference strength ($\Delta\sigma_R$ and $\Delta\tau_R$) and negative inverse slope (k) values are employed: standard values recommended by the IIW and those experimentally derived from uniaxial and pure torsional CA fatigue tests. Both standard and experimentally derived $\Delta\sigma_R$ and $\Delta\tau_R$ values are extrapolated based on $N_R = 2{\cdot}10^6$ cycles to failure, recalculated at a probability of survival (P_s) of 50%. The experimentally derived $\Delta\sigma_R$, $\Delta\tau_R$ (also commonly known as FAT), and k values are obtained via a linear regression model, assuming a log-normal distribution of number of cycles to failure. Both sets of constants are then applied to the reviewed critical plane models, including Findley's criterion, the CS approach, and the MWCM.

The standard S–N curves for welded joints exhibit characteristic knee points, where the negative inverse slope shifts at specific cycle counts. For uniaxial CA loading, the IIW defines a knee point at $N_{kp} = 10^7$ cycles to failure, with a pre-knee point negative inverse slope of $k = 3$. For pure torsional loading, the knee point is at $N_{kp} = 10^8$ cycles to failure, with a pre-knee point slope of $k_0 = 5$. After the knee point, the IIW recommends a postknee slope of $k^* = 22$ for both uniaxial and torsional CA loading [3]. In contrast, for VA loading, different post-knee point slopes are adopted: $k' = 5$ for uniaxial loading and $k_0' = 9$ for torsional loading, following Haibach's modification rule $(2k - 1)$ [3, 85]. These guidelines are applied in evaluating multiaxial fatigue criteria across all stress analysis methods, except when using the MWCM in combination with the TCD PM approach. For TCD PM, only standard recommended constants are used, as this method is derived based on ECs. The FAT values for both steel and aluminum welded joints are extrapolated at 5×10^6 cycles to failure. While the negative inverse slopes for steel are consistent with IIW recommendations, the pre-knee point slope for aluminum under uniaxial loading is adjusted to $k = 4.5$, reflecting its distinct fatigue behavior as specified in EC9 [2, 23, 37]. It is worth highlighting that for ease of comparison with the conventional reference stress range symbols recommended by the IIW and ECs, the normal and shear reference stresses in the tables are displayed as stress ranges at a P_s of 97.7% [1–3]. However, the accuracy of the evaluated critical plane criteria is calibrated using the recalculated reference stress ranges at a P_s of 50%, as previously noted.

To assess the accuracy of fatigue life predictions, the root mean square logarithmic error (RMSLE) is computed, followed by the derivation of a metric, T_{RMS}, as defined by Equations (15) and (16) [86, 87]. This metric quantifies the deviation between predicted and experimental results, providing a clear evaluation of the reliability for each criterion.

$$RMSLE = \sqrt{\frac{\sum_{i=1}^{n}\left[\left(\log\frac{N_{f(i)}}{N_{f,e(i)}}\right)^2\right]}{n}}, \tag{15}$$

$$T_{RMS} = 10^{RMSLE}, \tag{16}$$

where $N_{f(i)}$ denotes the experimentally observed number of cycles to failure for test i, $N_{f,e(i)}$ represents the estimated number of cycles to failure for the same test, and n refers to the total number of observations in each test series.

Predictions are classified as either conservative or nonconservative, where conservative estimates fall above the widest scatter band, based on a P_s of 97.7%, while nonconservative estimates fall below the scatter band, corresponding to P_s of 2.3%. Both standard and experimentally derived scatter bands are based on uniaxial and torsional tests under CA loading. To ensure consistency across results, only the widest scatter bands displayed in fatigue life graphs are used when determining the degree of conservatism, given the variability in experimentally derived scatter band sizes across different fatigue data series.

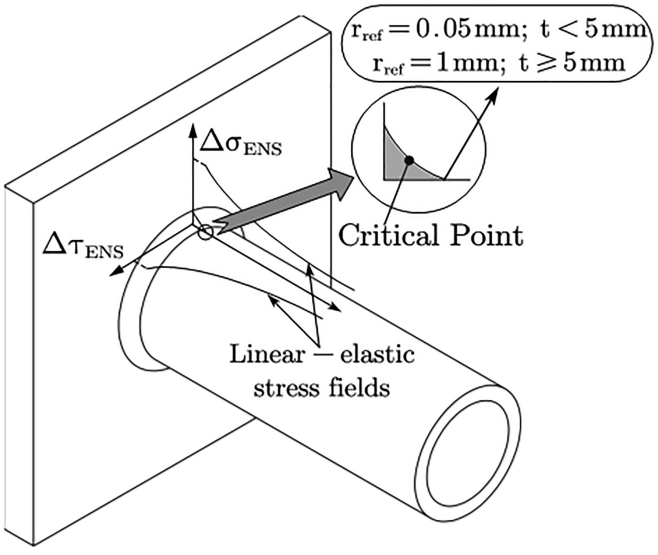

FIGURE 13 | Implementation of the effective notch stress (ENS) approach for different main reference thicknesses.

TABLE 3 | Summary of reanalyzed welded joints using *ENS approach* combined with critical plane criteria under *CA* and *VA* loading, detailing uniaxial and torsional reference fatigue strengths, joint geometries, materials, fatigue curve slopes, and data sources.

			Uniaxial curve slope, k						Torsional curve slope, k_0					
	$\Delta\sigma_{R,Ps=97.7\%}$[a] (MPa)		k (before knee point)[b]		k^* (after knee point)[b]		$\Delta\tau_{R,Ps=97.7\%}$[a] (MPa)		k_0 (before knee point)[c]		$k_0{}^*$ (after knee point)[c]			
Material (CA)	**IIW**	**Exp**[d]	**IIW**	**Exp**[d]	**IIW**	**Exp**[d]	**IIW**	**Exp**[d]	**IIW**	**Exp**[d]	**IIW**	**Exp**[d]	**Geometry**	**Reference**
UM StE 460[f]	225	362.6	3	4.4	22	22	160	221.0	5	4.9	22	22	Figure 4f	[26]
M StE 460[f]	225	332.1	3	4.6	22	22	160	—	5	—	22	22	Figure 4f	[73]
UM StE 460[f]	225	322.9	3	4.2	22	22	160	—	5	—	22	22	Figure 4b	[73]
StE 460[f]	225	365.1	3	4.2	22	22	160	321.5	5	7.3	22	22	Figure 4f	[79]
A519	225	192.8	3	5.4	22	22	160	145.6	5	3.7	22	22	Figure 4e	[78]
A519-A36[f]	225	295.2	3	3.8	22	22	160	183.1	5	5.5	22	22	Figure 4d	[77]
Fe 52 steel	225	40.0	3	2.3	22	22	160	53.2	5	3.5	22	22	Figure 4a	[66]
BS4360	630	—	5	—	22	22	250	—	7	—	22	22	Figure 4d	[65]
S340 + N, E355 + N	630	1114.0	5	6.1	22	22	250	551.1	7	6.6	22	22	Figure 4b	[72]
S340 + N, E355 + N[f]	630	243.0	5	2.9	22	22	250	191.3	7	3.6	22	22	Figure 4b	[72]
St 35 ($t = 1$ mm)	630	935.0	5	4.9	22	22	250	361.7	7	8.4	22	22	Figure 4b	[70]
St 35 ($t = 2$ mm)	630	1016.1	5	5.3	22	22	250	490.5	7	6.1	22	22	Figure 4b	[76]
6082-T6	71	140.5	3	6.9	22	22	63	84.5	5	6.2	22	22	Figure 4f	[74]
6060-T6[f]	180	406.0	5	5.5	22	22	90	—	7	—	22	22	Figure 4b	[68]
AW 6082	180	110.5	5	4.2	22	22	90	193.8	7	5.8	22	22	Figure 4b	[70]
AW 5042	180	215.7	5	4.1	22	22	90	194.9	7	5.9	22	22	Figure 4b	[70]

			Uniaxial curve slope, k						Torsional curve slope, k_0					
	$\Delta\sigma_{R,Ps=97.7\%}$[a] (MPa)		k (before knee point)[b]		k' (after knee point)[b]		$\Delta\tau_{R,Ps=97.7\%}$[a] (MPa)		k_0 (before knee point)[c]		k_0' (after knee point)[c]			
Material (VA)	**IIW**	**Exp**[d]	**IIW**	**Exp**[d]	**IIW**[e]	**Exp**[d]	**IIW**	**Exp**[d]	**IIW**	**Exp**[d]	**IIW**[e]	**Exp**[d]	**Geometry**	**Reference**
StE 460[f]	225	362.6	3	4.4	5	7.8	160	221.0	5	4.9	9	8.8	Figure 4f	[27]
StE 460[f]	225	365.1	3	3.9	5	6.8	160	321.5	5	7.3	9	13.6	Figure 4f	[79]
42CrMo4[f]	—	—	—	—	—	—	160	—	5	—	9	—	Figure 4b	[80]
6082-T6	71	140.5	3	6.9	5	12.8	63	42.3	5	6.3	9	11.6	Figure 4f	[75]

Abbreviations: M—machined; UM—unmachined.
[a]Reference normal and shear stresses extrapolated at two million cycles to failure, with $P_s = 97.7\%$.
[b]The knee point for the IIW in terms of normal stress corresponds to $N_{kp} = 10^7$ cycles.
[c]The knee point for the IIW in terms of shear stress corresponds to $N_{kp} = 10^8$ cycles.
[d]Exp refers to experimental data.
[e]Slopes (k' and k_0') suggested by the IIW for VA loading are derived from Haibach's modification ($2k - 1$), where k is the slope before the knee point.
[f]Stress relieved.

Regarding fatigue criteria calibration, both the CS approach and the MWCM are calibrated using uniaxial and pure torsional CA fatigue data. Because these data are used directly to calibrate the fatigue criteria, their accuracy under these specific loading conditions is not re-evaluated. Findley's criterion, however, is calibrated only with uniaxial fatigue data, so its uniaxial prediction accuracy is similarly excluded from further assessment. Performance under more complex multiaxial scenarios such as in-phase, out-of-phase, and VA loading are evaluated for all criteria.

In validating welded joints under VA loading with experimental constants, the average real damage sum, D_{real} values proposed by Eulitz and Sonsino are applied instead of the

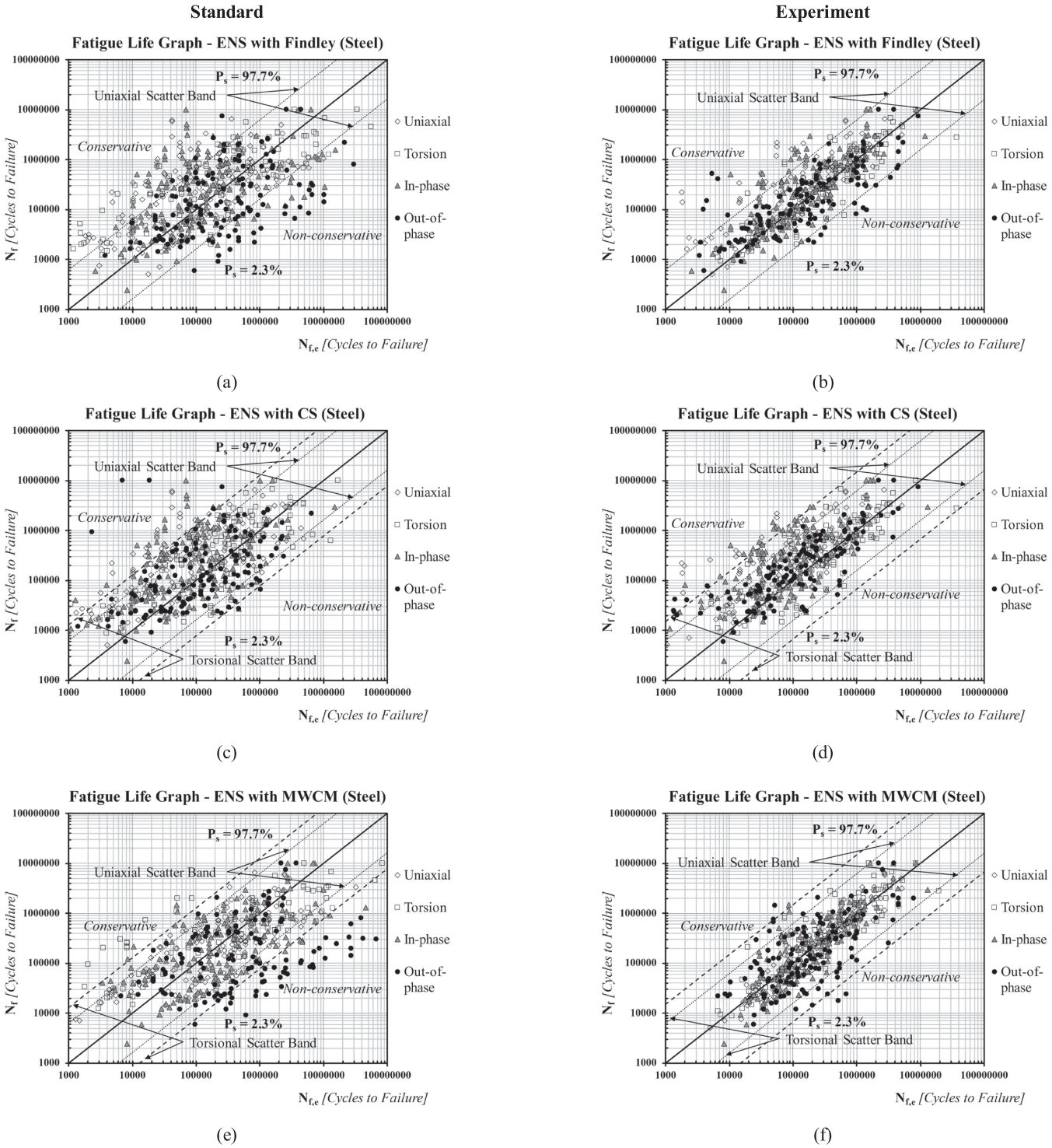

FIGURE 14 | Effective notch stress (ENS) approach: Fatigue life graphs for as-welded and stress-relieved *steel* welded joints using Findley's criterion (a,b), the CS method (c,d), and the MWCM (e,f) under *CA* fatigue loading, comparing standard and experimental reference strength based on $P_s = 50\%$.

standard 0.5 value recommended by ECs and IIW [88, 89]. Specifically, a D_{real} of 0.27 is applied for aluminum welded joints, and D_{real} of 0.45 for steel welded joints, providing more accurate prediction of fatigue life under both CA and VA loading conditions [88, 89].

4 | Reanalysis via the NS Approach

The NS approach calculates stresses based on the reference nominal cross-sectional area of welded joints. This method provides a straightforward and commonly used preliminary

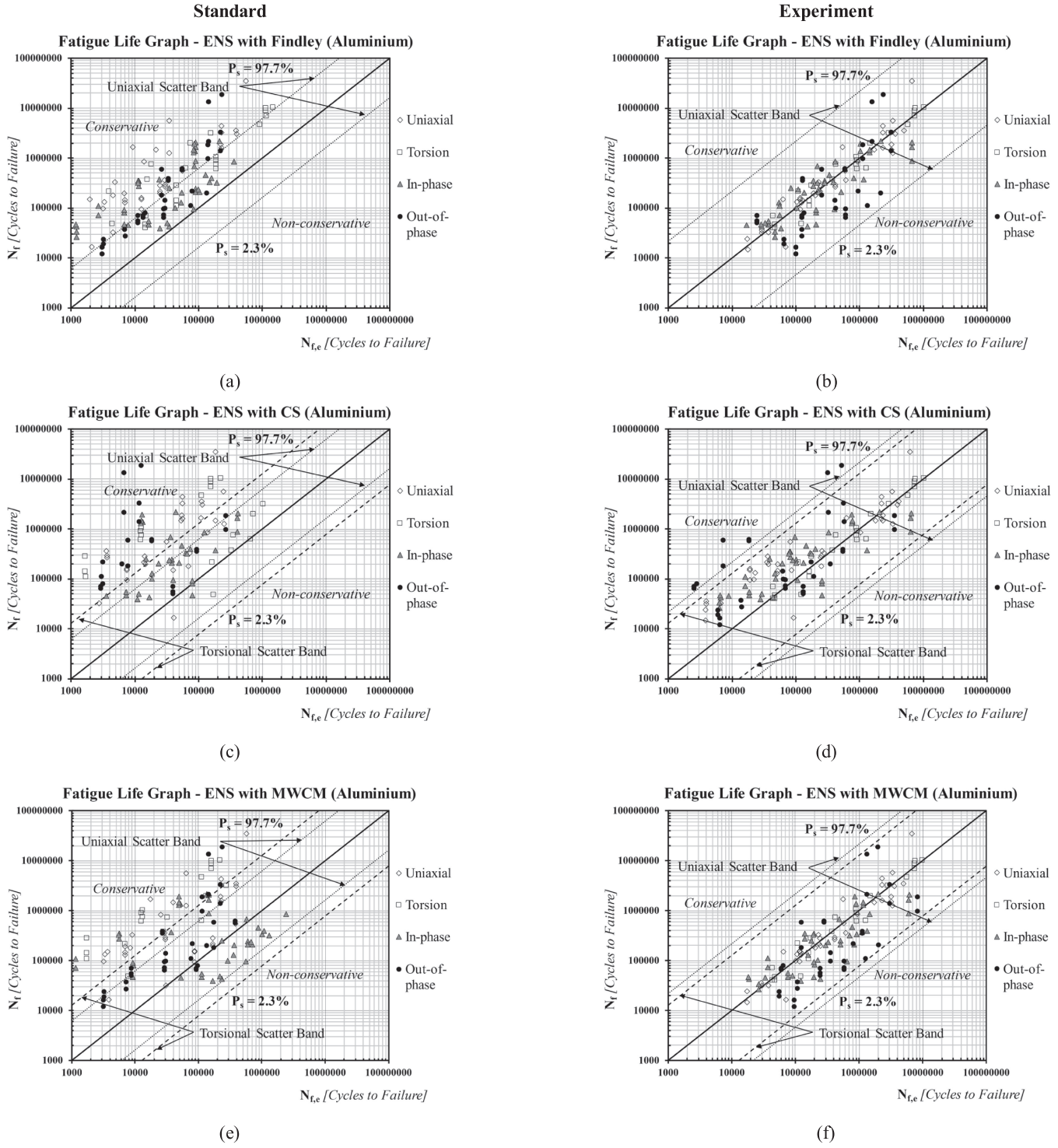

FIGURE 15 | Effective notch stress (ENS) approach: Fatigue life graphs for as-welded and stress-relieved *aluminum* welded joints using Findley's criterion (a,b), the CS approach (c,d), and the MWCM (e,f) under *CA* fatigue loading, comparing standard and experimental reference strength based on $P_s = 50\%$.

estimate before addressing more complex local stress effects [1–3, 40, 62, 82]. However, complications arise when welded geometries are intricate, making the definition of the reference area less clear.

Table 1 summarizes recalculated standard and experimental reference fatigue strengths at a P_s of 50%, along with corresponding k values for steel and aluminum welded joints under CA and VA loading using the NS approach. Fatigue life estimations using Findley's criterion, the CS approach, and the MWCM are illustrated in Figures 4 and 5.

For steel welded joints under CA loading, all fatigue criteria generally provided conservative fatigue life estimates with

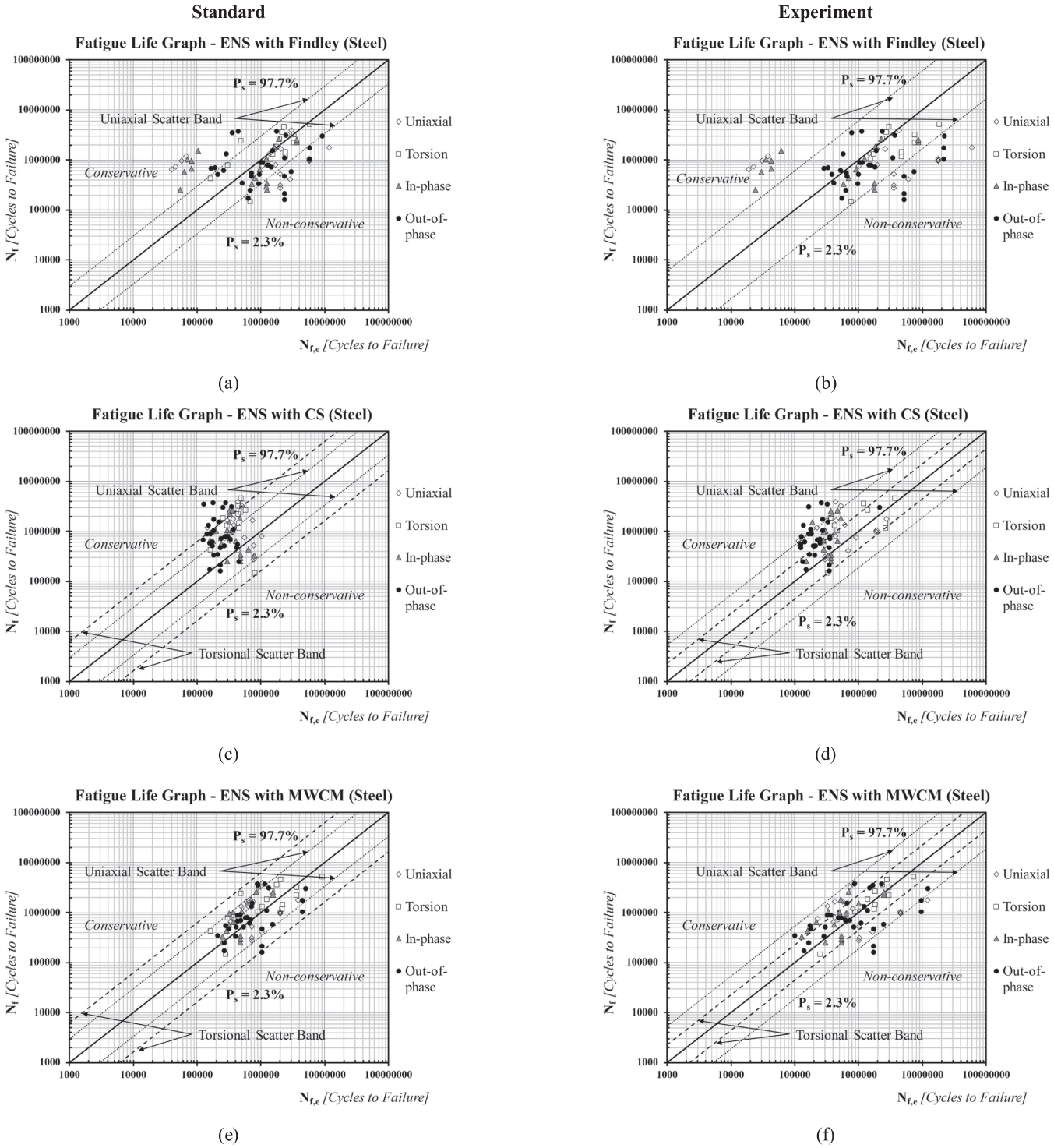

FIGURE 16 | Effective notch stress (ENS) approach: Fatigue life graphs for as-welded and stress-relieved *steel* welded joints using Findley's criterion (a,b), the CS approach (c,d), and the MWCM (e,f) under *VA* fatigue loading, comparing standard and experimental reference strength based on $P_s = 50\%$.

most data points falling within the widest scatter band, reflecting conservative yet safe estimates when using standard reference curves. However, the application of experimentally derived constants improved accuracy across all criteria by reducing the average percentage of conservative estimates, P_c, and nonconservative estimates, P_{NC}, as well as reducing the T_{RMS}. While the MWCM experiences a slight increase in T_{RMS}, the P_c and P_{NC} values remain low, highlighting its reliability when calibrated with experimental data. Overall, the differences in fatigue life estimations between the three criteria are minimal, and all provided satisfactory estimates under CA loading.

For aluminum welded joints under CA loading, a greater conservatism is observed compared to steel joints, particularly in out-of-phase loading conditions where the P_c value increases.

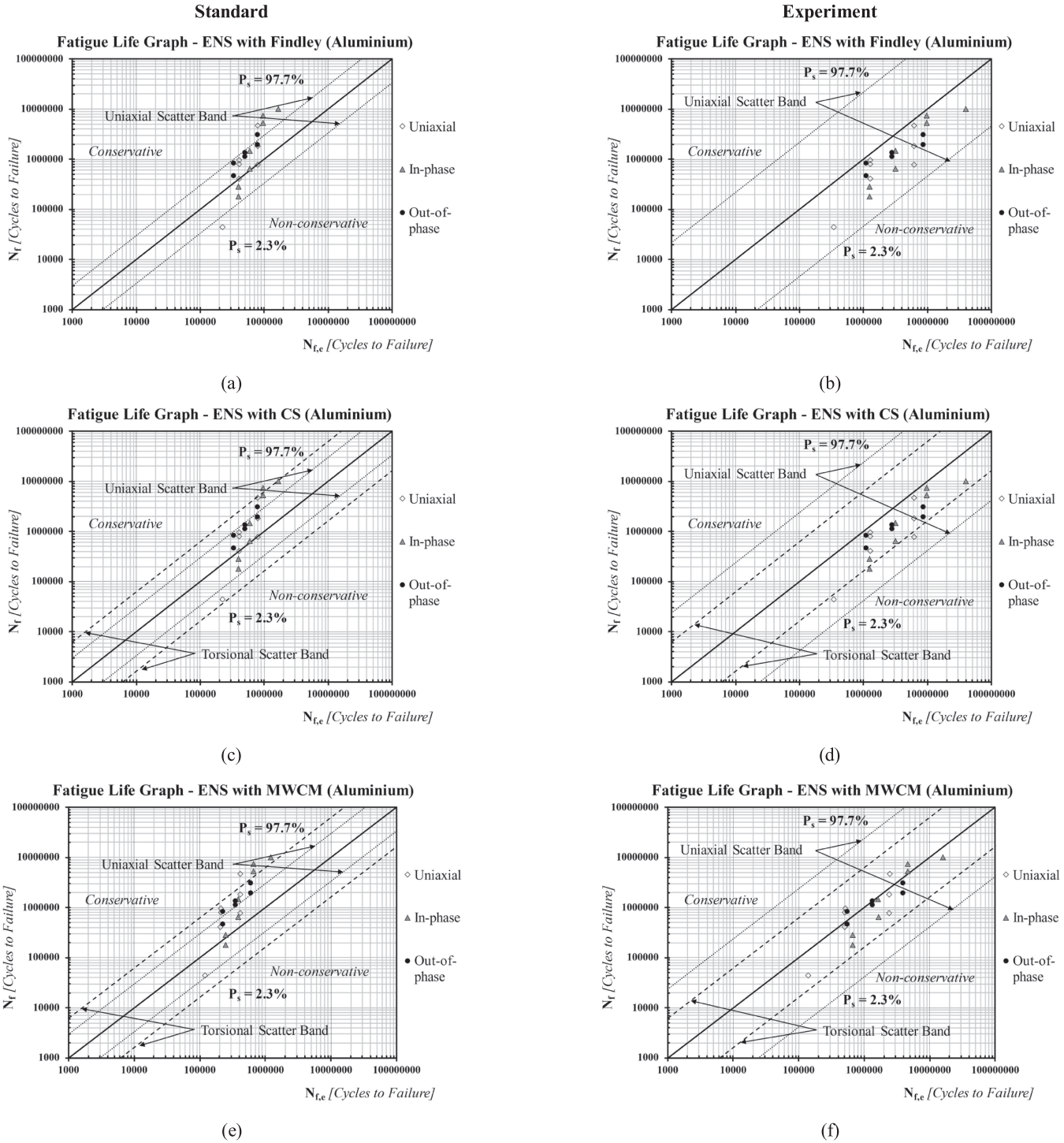

FIGURE 17 | Effective notch stress (ENS) approach: Fatigue life graphs for as-welded and stress-relieved *aluminum* welded joints using Findley's criterion (a,b), the CS approach (c,d), and the MWCM (e,f) under *VA* fatigue loading, comparing standard and experimental reference strength based on $P_s = 50\%$.

Additionally, aluminum joints show greater variability in fatigue life predictions, as indicated by their higher average T_{RMS} values relative to steel joints. Despite the increased scatter, all predictions remain conservative, ensuring the approach maintains an acceptable safety margin.

Under VA fatigue loading, fatigue life reanalysis results are shown in Figure 6 for steel welded joints and Figure 7 for aluminum welded joints. For steel joints, Findley's criterion exhibited substantial scatter, particularly at loading ratios of $R \geq 0$, resulting in highly conservative fatigue life estimates. This outcome is likely due to the inclusion of maximum normal stress in the calculation, leading to overly cautious estimates, especially because residual stresses from welding are already accounted for in the standard design reference curves [14, 15]. Furthermore, the stress relief treatments applied to most steel joints analyzed further increased the level of conservatism, as the adjustments introduced through enhancement factors proved insufficient to mitigate the effect. On the other hand, applying Findley's criterion with experimentally derived constants resulted in a higher level of nonconservative estimates. This discrepancy likely arises because the adopted criterion was calibrated using only uniaxial fatigue data, which may not fully capture the multiaxial fatigue behavior of steel welded joints [4, 15]. Consequently, Findley's criterion exhibited higher P_{NC} values compared to the CS approach and the MWCM.

Among the fatigue criteria, the MWCM delivered the most accurate fatigue life estimates for steel welded joints under VA loading, followed by the CS approach and Findley's criterion, as reflected by their respective average T_{RMS} values. As expected, VA loading introduced more scatter compared to CA loading, yet most fatigue life estimates remained conservative.

For aluminum welded joints under VA loading, the performance shifts, with the CS criterion showing more scatter in fatigue life estimates compared to Findley's criterion and the MWCM. The MWCM continues to deliver the most accurate results, followed by Findley, whose estimates generally fall within the scatter band but with a higher degree of conservatism.

Given the limited experimental data for aluminum welded joints under VA loading, further research is necessary to comprehensively validate these criteria [68–70, 75]. Nevertheless, the NS approach combined with multiaxial fatigue criteria provides safe and reliable fatigue life predictions for both steel and aluminum welded joints, regardless of loading complexity or joint condition. While experimental curves yield more accurate results, the standard reference curves remain effective for ensuring safe designs without introducing unnecessary conservatism.

5 | Reanalysis via the HSS Approach

The HSS approach, also known as the geometric stress approach, serves as an alternative to the NS approach for evaluating complex welded joint geometries. Unlike the NS approach, which only considers stresses at the nominal section, the HSS approach accounts for both membrane and shell bending stresses, but it excludes localized effects from the weld toe geometry [1–3, 36, 40, 62, 90–92]. However, its limitation is that it cannot be applied to critical regions at the weld root and is only suitable for weld toes [1–3, 36, 40, 62, 90–92]. In this study, a modified version of the HSS approach as originally proposed in [93] is employed as depicted in Figure 8. This modification deviates from the conventional definition that uses the maximum principal structural stress range at the crack initiation point [3, 62].

For multiaxial fatigue assessments, the modified HSS approach separates the stresses into two components: one perpendicular and the other parallel to the weld bead, determining both the normal and shear stress range on the critical plane [23, 37, 38, 93–95]. The rationale for this procedure lies in the observation that fatigue strength in materials weakened by notches with opening angles greater than 100° is primarily influenced by Modes I and III stress components, while Mode II contributions remain negligible due to their nonsingular nature [23, 37, 38, 93–95]. This method has been successfully applied and validated in previous studies involving welded joints [23, 37, 38, 93–95]. In this reanalysis, the normal and shear HSS stress components were calculated through finite element analysis (FEA) and extrapolated at reference points based on the reference plate thickness (t), specifically at $0.4t$ and $1.0t$, using fine mesh techniques based on Niemi's guidelines [62]. The resulting stresses were subsequently applied to the multiaxial fatigue criteria.

Table 2 outlines the essential characteristics of the reanalyzed steel and aluminum welded joints under CA and VA loading employing the HSS approach. It includes standard and experimental reference fatigue strengths recalculated at a P_s of 50%, along with their corresponding k values. The reanalysis results for steel and aluminum welded joints under CA loading using Findley's criterion, the CS approach, and the MWCM are shown in Figures 9 and 10. Across all criteria, most of the fatigue life predictions fall within the widest scatter band.

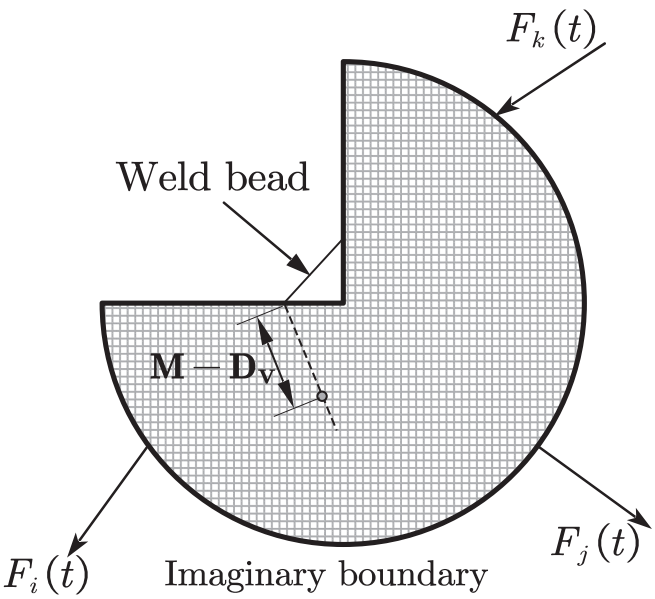

FIGURE 18 | Application of the theory of critical distances–point method (TCD PM) approach.

TABLE 4 | Summary of reanalyzed welded joints using the *TCD PM approach* with the MWCM under *CA* under *VA* loading, including uniaxial and torsional reference fatigue strengths, joint geometries, materials, fatigue curve slopes, and data sources.

Material (CA)	$\Delta\sigma_{R,Ps=97.7\%}$[a] (MPa)	Uniaxial curve slope, k		$\Delta\tau_{R,Ps=97.7\%}$[a] (MPa)	Torsional curve slope, k_0		Geometry	Reference
		k (before knee point)[b]	k^* (after knee point)[b]		k_0 (before knee point)[c]	$k_0{}^*$ (after knee point)[c]		
	TCD	TCD	TCD	TCD	TCD	TCD		
UM StE 460[e]	86	3	22	67	5	22	Figure 4f	[26]
M StE 460[e]	86	3	22	67	5	22	Figure 4f	[73]
UM StE 460[e]	86	3	22	67	5	22	Figure 4b	[73]
StE 460[e]	86	3	22	67	5	22	Figure 4f	[79]
A519	86	3	22	67	5	22	Figure 4e	[78]
A519-A36[e]	86	3	22	67	5	22	Figure 4d	[77]
Fe 52 steel	86	3	22	67	5	22	Figure 4a	[66]
BS4360	86	3	22	67	5	22	Figure 4d	[65]
S340 + N, E355 + N	86	3	22	67	5	22	Figure 4b	[72]
S340 + N, E355 + N[e]	86	3	22	67	5	22	Figure 4b	[72]
St 35 ($t = 1$ mm)	86	3	22	67	5	22	Figure 4b	[70]
St 35 ($t = 2$ mm)	86	3	22	67	5	22	Figure 4b	[76]
6082-T6	46	4.5	22	28	5	22	Figure 4f	[74]
6060-T6[e]	46	4.5	22	28	5	22	Figure 4b	[68]
AW 6082	46	4.5	22	28	5	22	Figure 4b	[70]
AW 5042	46	4.5	22	28	5	22	Figure 4b	[70]

Material (VA)	$\Delta\sigma_{R,Ps=97.7\%}$[a] (MPa)	Uniaxial curve slope, k		$\Delta\tau_{R,Ps=97.7\%}$[a] (MPa)	Torsional curve slope, k_0		Geometry	Reference
		k (before knee point)[b]	k' (after knee point)[b]		k_0 (before knee point)[c]	$k_0{}'$ (after knee point)[c]		
	IIW	TCD	TCD[d]	TCD	TCD	TCD[d]		
StE 460[e]	86	3	5	67	5	9	Figure 4f	[27]
StE 460[e]	71	3	5	67	5	9	Figure 4f	[79]
42CrMo4[e]	—	—	—	67	5	9	Figure 4b	[80]
6082-T6	46	4.5	8	28	5	9	Figure 4f	[75]

Abbreviations: M—machined; UM—unmachined.
[a]Reference normal and shear stresses extrapolated at five million cycles to failure, with a $P_s = 97.7\%$.
[b]The knee point for the TCD in terms of normal stress occurs at $N_{kp} = 10^7$ cycles to failure.
[c]The knee point for the TCD in terms of shear stress occurs at $N_{kp} = 10^8$ cycles to failure.
[d]Slopes (k' and k_0') for VA loading, as suggested by the TCD, are derived from Haibach's modification ($2k - 1$), where k is the slope before the knee point.
[e]Stress relieved.

Similar to the results of the NS approach, the use of experimentally derived constants significantly improved prediction accuracy, as indicated by lower T_{RMS} values and reduction of the average P_c.

All fatigue criteria showed improved performance when using the HSS approach, with lower T_{RMS} values compared to the NS approach for both steel and aluminum joints under CA loading. This trend holds true for VA loading as well, indicating that the HSS approach is more accurate due to its consideration of overall structural geometry. The differences between the criteria were again minimal, and all criteria performed satisfactorily when experimental constants were used.

For aluminum welded joints under CA loading, trends observed with the NS approach were evident, including increased conservatism and greater scatter compared to steel joints, as indicated by elevated P_c and T_{RMS} values. Although Findley's criterion and the CS method exhibited more scatter in their predictions, all estimates remained conservatively within safe margins.

Under VA loading, as illustrated in Figure 11, steel joints displayed greater scatter in fatigue life estimates compared to CA loading. In this case, the MWCM provided the most accurate fatigue life predictions, followed by the CS method, while Findley's criterion ranked last. Despite this, the HSS approach still resulted less scatter in fatigue life estimates overall compared to the NS approach. For aluminum joints under VA loading, depicted in Figure 12, the CS approach exhibited the most scatter, followed by Findley's criterion and the MWCM.

In summary, the application of multiaxial fatigue criteria using the HSS approach results in reliable fatigue life estimations for both steel and aluminum welded joints, particularly in cases where critical regions are located at the weld toe, regardless of the complexity of loading conditions.

6 | Reanalysis via the ENS Approach

The ENS approach addresses stress analysis by introducing a fictitious notch radius to prevent stress singularities at sharp features, such as weld toes or roots [3, 4, 40, 48, 63, 90, 96–100]. This method captures localized stress concentrations resulting from the weld profile geometry. Building on Neuber's microstructural support theory, Radaj proposed using a 1-mm effective notch radius for welded joints with a thickness of 5 mm or more, which accurately reflects the peak stress caused by notches [3, 4, 40, 48, 63, 90, 96–100]. This standardized radius allows for consistent fatigue assessments across various welded joint geometries, regardless of the actual radii at the weld toe or root.

However, for welded joints thinner than 5 mm, the IIW guidelines are inadequate. To address this, Sonsino introduced a fictitious notch radius of 0.05 mm, specifically designed for "thin and flexible" welded joints [63, 83, 98]. Sonsino also recommended adjusted k and reference fatigue strengths to account for the distinct fatigue behavior of these thinner joints [63, 83, 98]. This concept is depicted in Figure 13. In this analysis, joints with thicknesses below 5 mm are classified as thin and flexible, following Sonsino's recommendations, given the absence of IIW guidelines for ENS in this thickness range.

Table 3 provides key details of the reanalyzed steel and aluminum welded joints under CA and VA loading using the ENS approach, including standard and experimental reference fatigue strengths recalculated at a P_s of 50%, along with their corresponding *k* values.

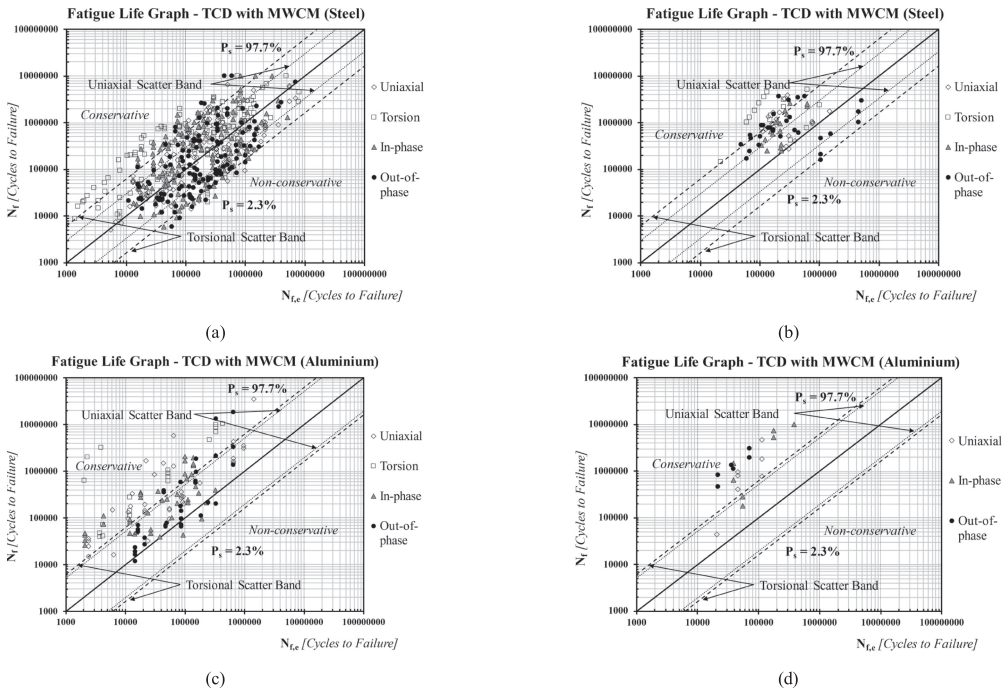

FIGURE 19 | The theory of critical distances–point method (TCD PM) approach: Fatigue life graphs for as-welded and stress-relieved *steel* (a,b) and *aluminum* (c,d) welded joints using the MWCM under *CA* (a,c) and *VA* (b,d) loading with standard reference strength based on $P_s = 50\%$.

TABLE 5 | Summary of P_{NC}, P_c, and T_{RMS} values from the reanalyses of *steel* joints under *CA* loading, using different critical plane criteria combined with various stress analysis approaches.

Multiaxial fatigue criterion	Condition	Stress analysis approaches	Standard[a]		Experimental[b]			
			P_{NC} (%)[c]	P_c (%)[d]	P_{NC} (%)[c]	P_c (%)[d]	$T_{RMS,Std}$[e]	$T_{RMS,Exp}$[f]
Findley	Uniaxial	NS	3.2	35.7	—	—	30.5	—
		HSS	0	36.6	—	—	22.3	—
		ENS	1.3	29.9	—	—	78.2	—
	Torsional	NS	6.8	27.1	4.2	0.8	16.8	7.2
		HSS	8.0	29.3	1.3	5.3	15.2	6.0
		ENS	2.7	21.6	1.8	4.5	44.0	6.4
	In-phase	NS	0.6	32.7	0	7.6	60.7	24.3
		HSS	0.8	11.1	3.2	15.9	14.9	10.0
		ENS	11.6	18.0	2.2	9.5	49.1	11.2
	Out-of-phase	NS	0.7	32.7	2.1	2.1	18.8	12.7
		HSS	4.0	15.0	13.0	9.0	8.0	9.0
		ENS	24.6	4.5	8.4	3.8	64.4	16.1
CS	Uniaxial	NS	3.2	36.9	—	—	30.8	—
		HSS	0	52.7	—	—	62.8	—
		ENS	2.1	33.1	—	—	97.6	—
	Torsional	NS	0.8	2.5	—	—	12.2	—
		HSS	0	5.3	—	—	9.6	—
		ENS	0.9	0.9	—	—	23.7	—
	In-phase	NS	0	20.7	0	0	43.5	14.2
		HSS	0.8	11.9	0	1.6	19.5	11.7
		ENS	0.6	8.7	0	5.6	51.8	65.7
	Out-of-phase	NS	0	15.6	1.4	0.0	19.5	11.9
		HSS	0	20.0	0	1.0	44.9	9.8
		ENS	1.5	3.7	0	3.9	60.9	14.3

(Continues)

The reanalysis results for steel and aluminum welded joints under CA loading applying Findley's criterion, the CS approach, and the MWCM are presented in Figures 14 and 15. For steel joints under CA loading, the ENS approach exhibited higher scatter and P_{NC} compared to the NS and HSS approaches, particularly when using standard reference curves. This increased variability and nonconservatism were largely driven by data from Shams' study on stress-relieved steel joints thinner than 5 mm.

Sonsino's recommendation, which employs a 0.05-mm fictitious notch radius, specifies k of 5 for uniaxial loading and k' of 7 for pure torsion reference curves, with standard reference strengths of 630 and 250 MPa, respectively [63, 83, 98]. However, experimental findings significantly deviated from these standards, revealing lower values which are 243 MPa for uniaxial and 191 MPa for pure torsional curves and steeper experimental slopes, with k values of 2.9 for uniaxial and 3.6 for torsional curves. These discrepancies contributed to the nonconservative fatigue predictions and increased scatter. Notably, this issue was predominantly observed in stress-relieved steel dataset from [72], while other thin and flexible joints remained within acceptable scatter ranges.

Under VA loading as illustrated in Figures 16 and 17, the performance of the fatigue criteria shifted. The ENS approach showed a higher scatter and increased P_{NC} with standard reference curves compared to the NS and HSS methods. However,

TABLE 5 | (Continued)

Multiaxial fatigue criterion	Condition	Stress analysis approaches	Standard[a]		Experimental[b]			
			P_{NC} (%)[c]	P_c (%)[d]	P_{NC} (%)[c]	P_c (%)[d]	$T_{RMS,Std}$[e]	$T_{RMS,Exp}$[f]
MWCM	Uniaxial	NS	8.3	23.6	—	—	13.8	—
		HSS	0	14.6	—	—	8.7	—
		ENS	5.7	6.4	—	—	19.2	—
		TCD	20.3	23.6	—	—	14.2	—
	Torsional	NS	4.2	7.6	—	—	12.0	—
		HSS	0	24.0	—	—	26.4	—
		ENS	1.0	11.7	—	—	66.0	—
		TCD	4.5	30.6	—	—	48.5	—
	In-phase	NS	2.8	7.3	0	0	15.7	15.7
		HSS	0	4.8	0	0.8	9.6	6.6
		ENS	3.7	2.5	0	0.6	25.3	6.3
		TCD	5.7	14.5	—	—	24.9	—
	Out-of-phase	NS	0	20.4	0	3.4	28.9	33.1
		HSS	0	7.0	0	0	8.4	10.5
		ENS	29.8	2.5	1.5	0.8	294.8	19.3
		TCD	4.6	6.9	—	—	18.4	—

[a]Reanalysis using constants derived from standard reference curves.
[b]Reanalysis using constants derived from experimental reference curves.
[c]P_{NC} represents the percentage of nonconservative estimates.
[d]P_c represents the percentage of conservative estimates.
[e]$T_{RMS,Std}$ quantifies the error in fatigue life predictions when using constants from standard curves.
[f]$T_{RMS,Exp}$ quantifies the error in fatigue life predictions when using constants from experimental curves.

applying experimental constants significantly improved accuracy, with most fatigue life estimates falling within acceptable scatter bands. This underscores the importance of experimental calibration in enhancing the predictive reliability of the ENS approach under complex loading conditions.

Despite its limitations with standard reference curves, the ENS approach remains an effective tool for fatigue life predictions when combined with multiaxial fatigue criteria and experimental calibration. The outlier case of stress-relieved thin and flexible joints from [72] highlights the need for individual testing to verify the applicability of recommended constants for unconventional thin and flexible welded joints. Overall, while more conservative, the ENS method provided safe and reliable estimations across a range of joint configurations and loading conditions, emphasizing its utility for structural design and analysis.

7 | Reanalysis via the Theory of Critical Distances (TCD) Approach

The TCD offers four primary variations, which include the Volume, Area, Line, and Point Method (PM) for calculating the effective stress, σ_{eff} [37, 47, 61, 101, 102]. These methods vary based on the size and shape of the integration domain used to postprocess the local linear-elastic stress field experienced by the material [37, 47, 61, 101, 102]. Among these formulations, the PM stands out as the simplest and most effective for predicting the fatigue life of welded joints, especially when used alongside the MWCM [23, 47, 103–105]. Therefore, this reanalysis adopts the TCD PM to compute effective stresses in conjunction with the MWCM. The implementation of the TCD PM approach is briefly described in Figure 18.

One of the main advantages of the TCD approach is that it eliminates the need for fictitious notch rounding, as required by the ENS approach, assuming zero weld root or toe radius [23, 47, 103, 105]. This simplification facilitates the analysis of complex geometries and reduces modeling time in FEA. The TCD is a localized stress analysis method designed to estimate multiaxial fatigue damage in welded connections by directly postprocessing linear-elastic stress fields around potential crack initiation sites [23, 47, 103, 105]. Fatigue damage assessment incorporates both the level of multiaxiality in the stress field through the MWCM and the influence of stress gradients via the TCD [23, 47, 103, 105].

The TCD PM is based on several key assumptions: It estimates fatigue damage under the premise of linear-elastic behavior of

TABLE 6 | Summary of P_{NC}, P_c, and T_{RMS} values from the reanalyses of *steel* joints under *VA* loading, using different critical plane criteria combined with various stress analysis approaches.

Multiaxial fatigue criterion	Condition	Stress analysis approaches	Standard[a]		Experimental[b]			
			P_{NC} (%)[c]	P_c (%)[d]	P_{NC} (%)[c]	P_c (%)[d]	$T_{RMS,Std}$[e]	$T_{RMS,Exp}$[f]
Findley	Uniaxial	NS	21.1	21.1	42.1	21.1	111.6	259.6
		HSS	5.3	31.6	42.1	21.1	153.0	257.5
		ENS	42.1	21.1	42.1	21.1	55.9	253.6
	Torsional	NS	0	80.0	41.7	33.3	60.3	24.1
		HSS	0	46.7	0	0	12.9	5.7
		ENS	6.7	6.7	0	0	5.8	8.8
	In-phase	NS	23.5	58.8	0	35.3	490.3	222.1
		HSS	0	52.9	0	35.3	383.6	110.4
		ENS	17.6	35.3	11.8	35.3	34.0	95.0
	Out-of-phase	NS	3.3	53.3	10.0	26.7	160.7	97.0
		HSS	6.7	43.3	23.3	23.3	128.5	64.6
		ENS	23.3	16.7	23.3	0	18.6	32.4
CS	Uniaxial	NS	0	36.8	36.8	68.4	20.3	34.3
		HSS	0	42.1	36.8	57.9	23.0	20.4
		ENS	0	36.8	0	42.1	18.0	15.6
	Torsional	NS	0	46.7	0	25.0	126.9	33.7
		HSS	0	20.0	0	36.4	24.0	50.3
		ENS	0	28.6	0	0	36.3	8.6
	In-phase	NS	0	17.6	0	0	23.0	11.5
		HSS	0	11.8	0	11.8	16.4	12.5
		ENS	0	17.6	0	17.6	19.5	15.6
	Out-of-phase	NS	0	16.7	3.6	21.4	19.0	28.5
		HSS	0	13.3	0	26.7	19.0	19.2
		ENS	0	26.7	0	23.3	92.2	29.9

(Continues)

the parent material and follows the notch bisector path for fatigue strength estimation, where stress components from the three fundamental modes are uncoupled [23, 47, 103, 105]. The critical distances, $M\text{-}D_v$, derived from the notch stress intensity factor (N-SIF) and EC standard curves for ground butt-welded steel and aluminum joints under uniaxial and pure torsional fatigue, are 0.5 mm for steel and 0.075 mm for aluminum [1, 2, 23, 47, 94, 103, 105, 106]. These critical distances are intrinsic material properties that remain constant, irrespective of geometry or stress complexity, enabling effective assessment of stress states at these points through FEA [23, 47, 103, 105].

Table 4 summarizes essential data from the reanalysis of steel and aluminum welded joints under both CA and VA loading using the TCD PM approach. This includes recalculated standard reference fatigue strengths at a P_s of 50%, as well as the corresponding k values. Figure 19 illustrates the reanalyzed fatigue life predictions using the TCD PM in conjunction with the MWCM.

The TCD PM consistently yields the most conservative fatigue life estimations, with P_{NC} values at 0% for most loading path scenarios, consistent with findings in Susmel's work [37, 61, 103]. However, it is important to note that the calibration of $M\text{-}D_v$ primarily relies on welded joints with main plate thicknesses between 6 and 24 mm, indicating that the TCD approach may not provide accurate fatigue life predictions for welded joints with thicknesses less than 5 mm [107].

TABLE 6 | (Continued)

Multiaxial fatigue criterion	Condition	Stress analysis approaches	Standard[a]		Experimental[b]			
			P_{NC} (%)[c]	P_c (%)[d]	P_{NC} (%)[c]	P_c (%)[d]	$T_{RMS,Std}$[e]	$T_{RMS,Exp}$[f]
MWCM	Uniaxial	NS	0	36.8	36.8	68.4	14.3	17.2
		HSS	0	42.1	36.8	57.9	26.2	12.6
		ENS	0	36.8	0	42.1	6.7	16.4
		TCD	0	57.9	—	—	37.9	—
	Torsional	NS	0	46.7	0	25.0	19.1	3.0
		HSS	0	20.0	0	36.4	11.9	1.8
		ENS	0	28.6	0	0	5.1	2.2
		TCD	33.3	80.0	—	—	291.6	—
	In-phase	NS	0	17.6	0	0	7.3	8.6
		HSS	0	11.8	0	11.8	22.8	5.4
		ENS	0	17.6	0	17.6	4.8	5.7
		TCD	0	11.8	—	—	22.3	—
	Out-of-phase	NS	0	16.7	3.6	21.4	9.1	10.4
		HSS	0	13.3	0	26.7	4.9	10.9
		ENS	0	26.7	0	23.3	6.7	12.0
		TCD	0	33.3	—	—	42.1	—

[a]Reanalysis using constants derived from standard reference curves.
[b]Reanalysis using constants derived from experimental reference curves.
[c]P_{NC} represents the percentage of nonconservative estimates.
[d]P_c represents the percentage of conservative estimates.
[e]$T_{RMS,Std}$ quantifies the error in fatigue life predictions when using constants from standard curves.
[f]$T_{RMS,Exp}$ quantifies the error in fatigue life predictions when using constants from experimental curves.

While the complexities of the calibration process and the assumption of zero weld root and toe radii contribute to the conservatism of the TCD PM, they also provide a necessary margin of safety. Practitioners can further enhance the accuracy of fatigue assessments by employing alternative reference curves and calibrating the critical distances, $M\text{-}D_v$ based on practical field experience, as suggested in relevant literature [23, 47]. Therefore, despite its increased conservatism and greater estimation error, as reflected higher T_{RMS} values, the TCD PM remains a reliable and practical option for evaluating multiaxial fatigue in both steel and aluminum welded joints when used in conjunction with the MWCM.

8 | Discussion

The reanalysis of P_{NC}, P_c, and T_{RMS} values, summarized in Tables 5–8, indicates that the multiaxial fatigue criteria and stress analysis approaches assessed in this study are suitable for designing welded joints. The choice of approach can be tailored to specific engineering constraints, with the HSS approach showing consistently strong performance across various cases.

For steel welded joints under CA loading, all criteria generally produced accurate and safe fatigue life predictions, with minimal variation. However, when considering VA loading, the MWCM demonstrated the most promising performance, followed by the CS criterion, while Findley's criterion showed the weakest performance with greater scatter and higher conservatism. This higher level of conservatism, especially in tests with loading ratios $R \geq 0$, can be linked to the fact that Findley's method indirectly accounts for mean stress via its maximum normal stress term. Because Findley's criterion was originally designed for unwelded components under multiaxial fatigue, its direct application to welded joints may require adjustments [14]. Specifically, replacing the maximum normal stress with the maximum normal stress range on the critical plane could enhance its accuracy. Further investigation is necessary to validate this adaptation, particularly for fatigue tests with $R \geq 0$. Additionally, the larger scatter observed in Findley's predictions may be due to the fact that it was calibrated using only uniaxial fatigue test data, whereas both the CS criterion and MWCM were calibrated with a broader dataset, including uniaxial and pure torsional fatigue data.

For aluminum welded joints, fatigue life predictions were generally more conservative and exhibited greater scatter compared to steel joints, under both CA and VA loading conditions. Although this is a known issue, it is important to emphasize that the conservatism arises primarily from the limited availability

TABLE 7 | Summary of P_{NC}, P_c, and T_{RMS} values from the reanalyses of *aluminum* joints under *CA* loading, using different critical plane criteria combined with various stress analysis approaches.

Multiaxial fatigue criterion	Condition	Stress analysis approaches	Standard[a]		Experimental[b]			
			P_{NC} (%)[c]	P_c (%)[d]	P_{NC} (%)[c]	P_c (%)[d]	$T_{RMS,Std}$[e]	$T_{RMS,Exp}$[f]
Findley	Uniaxial	NS	21.6	32.4	—	—	20.5	—
		HSS	0	64.7	—	—	45.1	—
		ENS	0	100	—	—	1505.3	—
	Torsional	NS	0	21.7	0	4.3	11.5	27.8
		HSS	0	85.7	0	0	156.5	3.7
		ENS	0	43.5	0	0	151.7	2.4
	In-phase	NS	0	58.1	0	7.0	24.0	57.5
		HSS	0	25.0	0	0	10.9	7.5
		ENS	0	53.5	0	0	198.2	6.0
	Out-of-phase	NS	0	30.3	0	12.1	33.7	154.6
		HSS	0	42.9	0	7.1	19.3	126.9
		ENS	0	42.4	0	0	120.6	23.0
CS	Uniaxial	NS	13.5	40.5	—	—	37.0	—
		HSS	0	82.4	—	—	100.6	—
		ENS	0	82.1	—	—	1364.6	—
	Torsional	NS	0	17.4	—	—	18.7	—
		HSS	0	71.4	—	—	12.7	—
		ENS	0	63.2	—	—	2264.0	—
	In-phase	NS	0	25.6	0	0	32.8	24.0
		HSS	0	14.3	0	0	24.1	10.0
		ENS	0	21.2	0	0	243.7	16.3
	Out-of-phase	NS	0	27.3	0	6.1	76.7	23.5
		HSS	0	35.7	0	7.1	774.7	56.4
		ENS	0	68.2	0	27.3	7620.3	98.4

(Continues)

of test data for aluminum joints [68–70, 75]. This highlights the need for further experimental studies to refine fatigue life predictions and enhance assessment accuracy. Interestingly, the performance of multiaxial fatigue criteria for aluminum joints differed from that observed for steel. In contrast to steel welded joints, where Findley's criterion was the most conservative, the CS criterion exhibited the highest level of conservatism and scatter for aluminum joints. This shift in behavior was particularly noticeable when standard constants were used for calibrating the criteria. The change in performance is likely attributable to differences in material ductility, as previously noted by Sonsino, which affect the orientation of the critical plane in fatigue analysis [27, 74, 75]. Based on these observations, it appears that the linear combination of shear and normal stress components produces more accurate results than the nonlinear combination for aluminum welded joints [4, 14, 15, 20, 37]. However, further testing on aluminum joints of various grade series and thicknesses subjected to multiaxial fatigue is needed to validate this hypothesis. Additional research would also clarify how material strength and ductility influence critical plane orientation, contributing to the development of a more robust fatigue model for aluminum welded joints under multiaxial fatigue loading.

When comparing the use of standard recommended constants, such as those provided by the IIW and ECs, to experimentally derived constants, it is evident that standard constants generally result in more conservative and scattered fatigue life estimates for both aluminum and steel welded joints. A notable exception was observed in stress-relieved steel welded joints of [72] under proportional and nonproportional loading, where nonconservative

TABLE 7 | (Continued)

Multiaxial fatigue criterion	Condition	Stress analysis approaches	Standard[a]		Experimental[b]			
			P_{NC} (%)[c]	P_c (%)[d]	P_{NC} (%)[c]	P_c (%)[d]	$T_{RMS,Std}$[e]	$T_{RMS,Exp}$[f]
MWCM	Uniaxial	NS	18.9	32.4	—	—	19.5	—
		HSS	0	41.2	—	—	33.2	—
		ENS	0	64.9	—	—	655.2	—
		TCD	18.9	48.6	—	—	157.9	—
	Torsional	NS	0	17.4	—	—	11.5	—
		HSS	0	71.4	—	—	153.6	—
		ENS	0	82.6	—	—	8461.3	—
		TCD	0	100	—	—	15829.0	—
	In-phase	NS	0	0.0	0	0	4.6	6.3
		HSS	0	3.6	0	0	7.7	8.0
		ENS	0	27.9	0	0	403.1	7.8
		TCD	0	39.5	—	—	104.2	—
	Out-of-phase	NS	0	21.2	0	6.1	36.3	25.3
		HSS	0	28.6	0	0	22.8	13.6
		ENS	0	18.2	0	0	80.5	30.0
		TCD	0	18.2	—	—	24.9	—

[a]Reanalysis using constants derived from standard reference curves.
[b]Reanalysis using constants derived from experimental reference curves.
[c]P_{NC} represents the percentage of nonconservative estimates.
[d]P_c represents the percentage of conservative estimates.
[e]$T_{RMS,Std}$ quantifies the error in fatigue life predictions when using constants from standard curves.
[f]$T_{RMS,Exp}$ quantifies the error in fatigue life predictions when using constants from experimental curves.

estimates occurred using the ENS approach with standard constants. This discrepancy is likely due to significant differences in the fatigue strength and negative inverse slope between experimentally derived curves and standard reference curves, as discussed in the ENS approach reanalysis section. In contrast, the use of experimentally derived curves significantly improved the accuracy of fatigue life predictions, as reflected by lower T_{RMS} values. This underscores the importance of conducting experimental investigations for nonconventional critical welded joints to properly calibrate multiaxial fatigue criteria and achieve accurate and reliable fatigue life estimations. Despite the higher error associated with standard constants, these errors typically result in conservative estimates, suggesting that the reference constants recommended in codes of practice are generally reliable and safe for use in most cases. This is particularly true for straightforward welded joint configurations that are fabricated using standard welding techniques covered by the codes. In scenarios where experimental studies are impractical or too costly, standard reference curves offer a dependable and safe alternative, providing a solid baseline for designing welded joints subjected to multiaxial fatigue loading.

In evaluating the performance of the multiaxial fatigue criteria under VA loading, the examined fatigue criteria demonstrated their ability to handle these complex loading scenarios, consistently producing conservative fatigue life estimates. However, VA loading resulted in increased variability and conservatism compared to CA loading, which is expected given the complexities associated with multiaxial fatigue under VA loading. Despite these challenges, the overall fatigue life predictions remained both safe and satisfactory, especially when experimental constants and average D_{real} values were applied for both aluminum and steel welded joints. The effectiveness of Findley's criterion and the CS approach in VA loading conditions can be partially attributed to the success of the CS counting method [21, 35]. This method proved effective in concurrently monitoring and counting both normal and shear stress signals, providing more accurate fatigue life estimations. Similarly, for the MWCM, the use of the MVM alongside conventional rainflow cycle counting proved a reliable strategy [59]. By determining the critical plane and calculating the effective shear stress range, the MVM enabled accurate fatigue life predictions across various stress analysis approaches when used with the MWCM.

The TCD PM, as the most conservative approach among the evaluated methods, provides a significant safety margin, particularly for welded joints with plate thicknesses between 6 and 24 mm, as discussed in the TCD approach section. However, for thinner plates with thicknesses below 5 mm, its reliance on

TABLE 8 | Summary of P_{NC}, P_c, and T_{RMS} values from the reanalyses of *aluminum* joints under *VA* loading, using different critical plane criteria combined with various stress analysis approaches.

Multiaxial fatigue criterion	Condition	Stress analysis approaches	Standard[a]		Experimental[b]			
			P_{NC} (%)[c]	P_c (%)[d]	P_{NC} (%)[c]	P_c (%)[d]	$T_{RMS,Std}$[e]	$T_{RMS,Exp}$[f]
Findley	Uniaxial	NS	14.3	0	0	0	11.6	116.4
		HSS	14.3	14.3	0	0	10.5	19.5
		ENS	14.3	14.3	0	0	11.1	19.3
	In-phase	NS	0	42.9	0	0	15.8	6.6
		HSS	0	42.9	0	0	40.3	7.0
		ENS	0	42.9	0	0	20.3	19.0
	Out-of-phase	NS	0	16.7	0	0	5.7	2.9
		HSS	0	16.7	0	0	11.5	3.2
		ENS	0	16.7	0	0	8.6	9.1
CS	Uniaxial	NS	14.3	71.4	0	0	159.2	36.6
		HSS	14.3	42.9	0	14.3	82.3	84.5
		ENS	14.3	14.3	0	0.0	11.1	19.3
	In-phase	NS	0	42.9	0	42.9	84.3	283.7
		HSS	0	42.9	0	0	111.6	67.8
		ENS	0	14.3	0	0	20.3	19.0
	Out-of-phase	NS	0	50.0	0	16.7	55.3	246.5
		HSS	0	66.7	0	0	84.4	92.2
		ENS	0	0	0	0	8.6	9.1
MWCM	Uniaxial	NS	14.3	14.3	0	0	14.3	5.3
		HSS	0	57.1	0	0	35.9	5.5
		ENS	0	57.1	0	0	26.3	5.4
		TCD	0	85.7	—	—	423.8	
	In-phase	NS	0	14.3	0	0	16.9	6.0
		HSS	0	42.9	0	0	55.8	5.3
		ENS	0	42.9	0	0	35.9	5.4
		TCD	0	57.1	—	—	920.4	—
	Out-of-phase	NS	0	0	0	0	5.8	3.1
		HSS	0	0	0	0	25.8	2.6
		ENS	0	0	0	0	18.3	2.3
		TCD	0	100	—	—	2920.9	—

[a]Reanalysis using constants derived from standard reference curves.
[b]Reanalysis using constants derived from experimental reference curves.
[c]P_{NC} represents the percentage of nonconservative estimates.
[d]P_c represents the percentage of conservative estimates.
[e]$T_{RMS,Std}$ quantifies the error in fatigue life predictions when using constants from standard curves.
[f]$T_{RMS,Exp}$ quantifies the error in fatigue life predictions when using constants from experimental curves.

standard calibration methods, such as those in EC3 and EC9, may result in less accurate fatigue life predictions. This inherent conservatism, coupled with simplifying assumptions like zero weld root and toe radii, contributes to increased variability in the estimates. To enhance its applicability, particularly for non-standard joint configurations, future research should explore the

refinement of calibration procedures through the use of alternative reference curves and empirical fatigue data. Nonetheless, the TCD PM remains a reliable option for multiaxial fatigue assessment when paired with the MWCM, particularly in cases where safety is a priority.

Overall, this quantitative review confirms the effectiveness and validity of alternative critical plane approaches, including Findley's criterion, the CS approach, and the MWCM, in combination with various stress analysis methods, for plate thicknesses of up to 10 mm. These approaches offer a valuable alternative to the standard interaction equations recommended by codes such as the IIW and ECs [1–3, 5]. By recognizing the unique strengths and characteristics of each fatigue criterion and joint type, engineers are better equipped to make informed decisions, leading to safer and more efficient design solutions to address multiaxial fatigue challenges.

Nomenclature

$\Delta\sigma_x$	normal stress range in x direction
$\Delta\tau_{xy}$	shear stress range in xy direction
$\Delta\sigma$	normal stress range
$\Delta\tau$	shear stress range
$\Delta\sigma_n$	normal stress range relative to the critical plane
$\Delta\sigma_{eq}$	equivalent normal stress range for VA loading
$\Delta\tau_{eq}$	equivalent shear stress range for VA loading
$\Delta\sigma_R$	reference normal stress extrapolated at N_R cycles to failure
$\Delta\tau_R$	reference shear stress extrapolated at N_R cycles to failure
$\Delta\sigma_{R,Ps=97.7\%}$	reference normal stress extrapolated at N_R cycles recalculated for a P_s of 97.7%
$\Delta\tau_{R,Ps=97.7\%}$	reference shear stress extrapolated at N_R cycles recalculated for a P_s of 97.7%
$\Delta\sigma_{NS}$	effective normal stress range derived from nominal stress approach
$\Delta\sigma_{HSS}$	effective normal stress range derived from hot-spot stress approach
$\Delta\sigma_{ENS}$	effective normal stress range derived from effective notch stress approach
$\Delta\tau_{NS}$	effective shear stress range derived from nominal stress approach
$\Delta\tau_{HSS}$	effective shear stress range derived from hot-spot stress approach
$\Delta\tau_{ENS}$	effective shear stress range derived from effective notch stress approach
$\Delta\sigma_{eff}$	effective stress range
$\sigma_{\min}$	minimum normal stress
$\sigma_{\max}$	maximum normal stress
$\tau_{\min}$	minimum shear stress
$\tau_{\max}$	maximum shear stress
σ_m	mean normal stress
σ_u	ultimate tensile strength
$\Delta\sigma_{find}$	effective stress range derived from Findley's criterion
$\Delta\sigma_{CS}$	effective stress range derived from CS criterion
$\Delta\tau_{MWCM}$	effective stress range derived from MWCM criterion
$\Delta\sigma_{R=-1}$	fully reversed uniaxial reference stress range extrapolated at N_R cycles to failure
$\Delta\tau_{R=-1}$	fully reversed torsional reference stress range extrapolated at N_R cycles to failure
$\Delta\tau_{R,MWCM}$	MWCM reference shear stress range determined at N_R cycles to failure
$\tau_{MV}(t)$	shear stress resolved along maximum variance direction at any instant of time
τ_m	mean shear stress
T	time interval
f	fatigue damage parameter for Findley's criterion
β	material constant for Findley's criterion
δ	off angle between the normal to critical plane and the weighted average direction of the first principal stress for CS criterion
ρ_w	MWCM effective critical plane stress ratio for welded joints
$\rho_{w,lim}$	limit of the MWCM effective critical plane stress ratio
R	stress ratio
t	welded joint plate thickness under loading
$\sigma_{0.4t}$	stress state at $0.4t$ according to the hot-spot stress linear extrapolation method
$\sigma_{1.0t}$	stress state at $1.0t$ according to the hot-spot stress linear extrapolation method
k	negative inverse slope for uniaxial fatigue S–N curve
k_0	negative inverse slope for pure torsional fatigue S–N curve
k^*	negative inverse slope for uniaxial S–N curve after knee point under CA
$k_0{}^*$	negative inverse slope for pure torsional S–N curve after knee point under CA
k'	negative inverse slope for uniaxial S–N curve after knee point under VA
$k_0{}'$	negative inverse slope for pure torsional S–N curve after knee point under VA
k_τ	negative inverse slope for MWCM
D_{real}	real damage sum derived experimentally
N_R	reference number of cycles to failure
N_f	experimental number of cycles to failure
$N_{f,e}$	estimated number of cycles to failure
$N_{f(i)}$	experimental number of cycles to failure for test i
$N_{f,e(i)}$	estimated number of cycles to failure for test i
N_{kp}	number of cycles at knee point (location of knee point)
n	total number of observations in each test series
$f(R)$	enhancement factor for stress-relieved welded joints
RMSLE	root mean squared logarithmic error
T_{RMS}	metric to quantify the performance and accuracy of each criterion, that is, lower values indicate better performance

$T_{RMS,Std}$	metric to quantify the performance of each criterion when using constants from standard curves
$T_{RMS,Exp}$	metric to quantify the performance of each criterion when using constants from experimental curves
P_{NC}	percentage of nonconservative estimates
P_c	percentage of conservative estimates
P_s	probability of survival
r_{ref}	fictitious reference notch radius for ENS approach
$M\text{-}D_v$	critical distance for TCD PM
CS	Carpinteri–Spagnoli
MWCM	Modified Wöhler Curve Method
SWT	Smith, Watson, and Topper
EESH	effective equivalent stress hypothesis
CA	constant amplitude
VA	variable amplitude
NS	nominal stress
HSS	hot-spot stress
ENS	effective notch stress
TCD	Theory of Critical Distances
PM	Point Method
IIW	International Institute of Welding
EC3	Eurocode 3
EC9	Eurocode 9
ECs	Eurocodes
ASTM	American Society for Testing and Materials
FKM	Forschungskuratorium Maschinenbau
MVM	maximum variance method
HAZ	heat-affected zone
FEA	finite element analysis
N-SIF	notch stress intensity factor

9 | Conclusions

This comprehensive quantitative review of various stress-based critical plane criteria, specifically Findley's criterion, the CS approach, and the MWCM addresses the multiaxial fatigue of aluminum and steel welded joints under CA and variable amplitude VA loading. The key findings are summarized as follows:

- For steel welded joints, all criteria demonstrated satisfactory performance under CA loading, with minimal differences in the accuracy of fatigue life estimations. For VA loading, the MWCM showed the best performance, followed by CS, while Findley's criterion was more conservative and scattered due to its indirect treatment of mean stress via the maximum normal stress term.
- Fatigue predictions for aluminum joints displayed greater conservatism and scatter compared to steel, especially with the CS criterion. This underscores the need for additional experimental data to improve accuracy for aluminum joints.
- Standard calibration constants generally result in conservative estimates but offer a safe baseline when experimental data is unavailable [1–3]. However, using experimentally derived constants significantly improve fatigue life estimation accuracy, particularly for nonconventional joint configurations.
- The TCD PM combined with MWCM, the most conservative stress analysis approach, could benefit from refinement to improve accuracy, particularly for thinner and more flexible ($t < 5$ mm) or nonstandard welded joint configurations.
- The critical plane criteria assessed, namely, Findley's criterion, the CS approach, and the MWCM generally provide accurate and reliable assessments of multiaxial fatigue in welded joints. These criteria serve as viable alternatives to conventional interaction equation criteria outlined in codes such as the IIW and ECs, especially when experimentally calibrated constants are employed.
- While these fatigue criteria have demonstrated overall effectiveness, further research is crucial to refine their application to aluminum welded joints, particularly under CA and VA multiaxial loading. Compared to steel welded joints, studies on aluminum welded joints across various grade series and thicknesses remain limited. Addressing this gap will enhance the accuracy and reliability of fatigue life estimations and ensure the criteria's robustness to these less-explored scenarios.

Data Availability Statement

The data that support the findings of this study are available from the corresponding author upon reasonable request.

References

1. Anon, "Eurocode 3: Design of Steel Structures—Part 1–9: Fatigue," (2005).

2. Anon, "Eurocode 9: Design of Aluminium Structures—Part 1–3: Structures Susceptible to Fatigue," (2007).

3. A. Hobbacher, *Recommendations for Fatigue Design of Welded Joints and Components*, vol. 47 (Cham, Switzerland: Springer, 2016).

4. M. M. Pedersen, "Multiaxial Fatigue Assessment of Welded Joints Using the Notch Stress Approach," *International Journal of Fatigue* 83 (2016): 269–279.

5. C. T. Ng, C. M. Sonsino, and L. Susmel, "Multiaxial Fatigue Assessment of Welded Joints: A Review of Eurocode 3 and International Institute of Welding Criteria With Different Stress Analysis Approaches," *Fatigue and Fracture of Engineering Materials and Structures* 47 (2024): 2616–2649.

6. W. Fricke, "Fatigue Analysis of Welded Joints: State of Development," *Marine Structures* 16 (2003): 185–200.

7. C. M. Sonsino, "Multiaxial Fatigue Assessment of Welded Joints–Recommendations for Design Codes," *International Journal of Fatigue* 31 (2009): 173–187.

8. K. N. Smith, "A Stress-Strain Function for the Fatigue of Metals," *Journal of Materials* 5 (1970): 767–778.

9. T. Łagoda, S. Vantadori, K. Głowacka, M. Kurek, and K. Kluger, "Using the Smith-Watson-Topper Parameter and Its Modifications to Calculate the Fatigue Life of Metals: The State-of-the-Art," *Materials (Basel)* 15 (2022): 3481.

10. M. W. Brown and K. J. Miller, "A Theory for Fatigue Failure Under Multiaxial Stress-Strain Conditions," *Proceedings of the Institution of Mechanical Engineers* 187 (1973): 745–755.

11. M. W. Brown and K. J. Miller, "Initiation and Growth of Cracks in Biaxial Fatigue," *Fatigue and Fracture of Engineering Materials and Structures* 1 (1979): 231–246.

12. A. Fatemi and D. F. Socie, "A Critical Plane Approach to Multiaxial Fatigue Damage Including Out-of-Phase Loading," *Fatigue and Fracture of Engineering Materials and Structures* 11 (1988): 149–165.

13. D. F. Socie, "Multiaxial Fatigue Damage Models," *Journal of Engineering Materials and Technology* 109 (1987): 293–298.

14. W. N. Findley, "A Theory for the Effect of Mean Stress on Fatigue of Metals Under Combined Torsion and Axial Load or Bending," *Journal of Engineering for Industry* 81 (1959): 301–305.

15. Ø. A. Bruun and G. Härkegård, "A Comparative Study of Design Code Criteria for Prediction of the Fatigue Limit Under In-Phase and Out-of-Phase Tension–Torsion Cycles," *International Journal of Fatigue* 73 (2015): 1–16.

16. T. Matake, "An Explanation on Fatigue Limit Under Combined Stress," *Bulletin of JSME* 20 (1977): 257–263.

17. D. L. McDiarmid, "A General Criterion for High Cycle Multiaxial Fatigue Failure," *Fatigue and Fracture of Engineering Materials and Structures* 14 (1991): 429–453.

18. D. L. McDiarmid, "A Shear Stress Based Critical-Plane Criterion of Multiaxial Fatigue Failure for Design and Life Prediction," *Fatigue and Fracture of Engineering Materials and Structures* 17 (1994): 1475–1484.

19. K. Dang-Van, "Macro-Micro Approach in High-Cycle Multiaxial Fatigue," in *Advances in Multiaxial Fatigue*, eds. D. McDowell and J. Ellis (West Conshohocken, PA: ASTM International, 1993).

20. A. Carpinteri, A. Spagnoli, and S. Vantadori, "Multiaxial Fatigue Life Estimation in Welded Joints Using the Critical Plane Approach," *International Journal of Fatigue* 31 (2009): 188–196.

21. A. Carpinteri, A. Spagnoli, and S. Vantadori, "A Multiaxial Fatigue Criterion for Random Loading," *Fatigue and Fracture of Engineering Materials and Structures* 26 (2003): 515–522.

22. Carpinteri, Brighenti, and Spagnoli, "A Fracture Plane Approach in Multiaxial High-Cycle Fatigue of Metals," *Fatigue sand Fracture of Engineering Materials and Structures* 23 (2000): 355–364.

23. L. Susmel, *Multiaxial Notch Fatigue* (Cambridge, UK: Elsevier, 2009).

24. B. Li, L. Reis, and M. De Freitas, "Comparative Study of Multiaxial Fatigue Damage Models for Ductile Structural Steels and Brittle Materials," *International Journal of Fatigue* 31 (2009): 1895–1906.

25. S.-P. Zhu, Z.-Y. Yu, J. Correia, A. De Jesus, and F. Berto, "Evaluation and Comparison of Critical Plane Criteria for Multiaxial Fatigue Analysis of Ductile and Brittle Materials," *International Journal of Fatigue* 112 (2018): 279–288.

26. C. M. Sonsino, "Multiaxial Fatigue of Welded Joints Under In-Phase and Out-of-Phase Local Strains and Stresses," *International Journal of Fatigue* 17 (1995): 55–70.

27. C. M. Sonsino and M. Kueppers, "Multiaxial Fatigue of Welded Joints Under Constant and Variable Amplitude Loadings," *Fatigue and Fracture of Engineering Materials and Structures* 24 (2001): 309–327.

28. S. Macha, "Energy Criteria of Multiaxial Fatigue Failure," *Fatigue and Fracture of Engineering Materials and Structures* 22 (1999): 1053–1070.

29. P. Foti and F. Berto, "Fatigue Assessment of High Strength Welded Joints Through the Strain Energy Density Method," *Fatigue and Fracture of Engineering Materials and Structures* 43 (2020): 2694–2702.

30. G. Glinka, G. Shen, and A. Plumtree, "A Multiaxial Fatigue Strain Energy Density Parameter Related to the Critical Fracture Plane," *Fatigue and Fracture of Engineering Materials and Structures* 18 (1995): 37–46.

31. F. Ellyin, "Cyclic Strain Energy Density as a Criterion for Multiaxial Fatigue Failure," *Biaxial and Multiaxial Fatigue* 3 (1989): 571–583.

32. L. Gan, H. Wu, and Z. Zhong, "Multiaxial Fatigue Life Prediction Based on a Simplified Energy-Based Model," *International Journal of Fatigue* 144 (2021): 106036.

33. P. Lazzarin, P. Livieri, F. Berto, and M. Zappalorto, "Local Strain Energy Density and Fatigue Strength of Welded Joints Under Uniaxial and Multiaxial Loading," *Engineering Fracture Mechanics* 75 (2008): 1875–1889.

34. J. Papuga, "A Survey on Evaluating the Fatigue Limit Under Multiaxial Loading," *International Journal of Fatigue* 33 (2011): 153–165.

35. N. D. Bibbo, J. Baumgartner, and V. Arora, "Comparative Study of Critical Plane Fatigue Criteria on Multiaxial Variable Amplitude Loaded Welded Test Specimens," *International Journal of Fatigue* 158 (2022): 106670.

36. J. Mei, P. Dong, S. Xing, et al., "An Overview and Comparative Assessment of Approaches to Multi-Axial Fatigue of Welded Components in Codes and Standards," *International Journal of Fatigue* 146 (2021): 106144.

37. L. Susmel, "Four Stress Analysis Strategies to Use the Modified Wöhler Curve Method to Perform the Fatigue Assessment of Weldments Subjected to Constant and Variable Amplitude Multiaxial Fatigue Loading," *International Journal of Fatigue* 67 (2014): 38–54.

38. L. Susmel, "Three Different Ways of Using the Modified Wöhler Curve Method to Perform the Multiaxial Fatigue Assessment of Steel and Aluminium Welded Joints," *Engineering Failure Analysis* 16 (2009): 1074–1089.

39. L. Susmel and H. Askes, "Modified Wöhler Curve Method and Multiaxial Fatigue Assessment of Thin Welded Joints," *International Journal of Fatigue* 43 (2012): 30–42.

40. D. Radaj, "Review of Fatigue Strength Assessment of Nonwelded and Welded Structures Based on Local Parameters," *International Journal of Fatigue* 18 (1996): 153–170.

41. M. Bäckström and G. Marquis, "A Review of Multiaxial Fatigue of Weldments: Experimental Results, Design Code and Critical Plane Approaches," *Fatigue and Fracture of Engineering Materials and Structures* 24 (2001): 279–291.

42. M. M. Pedersen, *Introduction to Metal Fatigue. No Tech Rep ME-TR-11* (Aarhus, Denmark: Aarhus University, 2018): 91.

43. G. Marquis, M. Bäckström, and A. Siljander, "Multiaxial Fatigue Damage Parameters for Welded Joints: Design Code and Critical Plane Approaches," in *1st North European Engineering and Science Conference (NESCO I)* (Cradley Heath: Engineering Materials Advisory Services EMAS, 1997).

44. A. Carpinteri, E. Macha, R. Brighenti, and A. Spagnoli, "Expected Principal Stress Directions Under Multiaxial Random Loading. Part I: Theoretical Aspects of the Weight Function Method," *International Journal of Fatigue* 21 (1999): 83–88.

45. A. Carpinteri, R. Brighenti, E. Macha, and A. Spagnoli, "Expected Principal Stress Directions Under Multiaxial Random Loading. Part II: Numerical Simulation and Experimental Assessment Through the Weight Function Method," *International Journal of Fatigue* 21 (1999): 89–96.

46. L. Susmel, R. Tovo, and D. Benasciutti, "A Novel Engineering Method Based on the Critical Plane Concept to Estimate the Lifetime of Weldments Subjected to Variable Amplitude Multiaxial Fatigue Loading," *Fatigue and Fracture of Engineering Materials and Structures* 32 (2009): 441–459.

47. L. Susmel, "The Modified Wöhler Curve Method Calibrated by Using Standard Fatigue Curves and Applied in Conjunction With the Theory of Critical Distances to Estimate Fatigue Lifetime of Aluminium Weldments," *International Journal of Fatigue* 31 (2009): 197–212.

48. I. Al Zamzami and L. Susmel, "On the Use of Hot-Spot Stresses, Effective Notch Stresses and the Point Method to Estimate Lifetime of Inclined Welds Subjected to Uniaxial Fatigue Loading," *International Journal of Fatigue* 117 (2018): 432–449.

49. L. Susmel and P. Lazzarin, "A Bi-Parametric Wöhler Curve for High Cycle Multiaxial Fatigue Assessment," *Fatigue and Fracture of Engineering Materials and Structures* 25 (2002): 63–78.

50. T. E. Langlais, J. H. Vogel, and T. R. Chase, "Multiaxial Cycle Counting for Critical Plane Methods," *International Journal of Fatigue* 25 (2003): 641–647.

51. ASTM Standard, *E1049–85 (Reapproved 2017) Standard Practices for Cycle Counting in Fatigue Analysis*. Tech. Rep. (West Conshohocken, PA: ASTM International, 2017).

52. Y. L. Lee and J. Pan, *Fatigue Testing and Analysis: Theory and Practice*, vol. 106 (Oxford, UK: Elsevier, 2005).

53. Y.-L. Lee and T. Tjhung, "Rainflow Cycle Counting Techniques," in *Metal Fatigue Analysis Handbook: Practical Problem-Solving Techniques for Computer-Aided Engineering* (Oxford, UK: Butterworth-Heinemann, 2011): 89.

54. M. Matsuishi, *Fatigue of Metals Subjected to Varying Stress* (Fukuoka, Japan: Japan Society of Mechanical Engineering, 1968).

55. T. Endo, M. Matsuishi, K. Mitsunaga, K. Kobayashi, and K. Takahashi, "Rain Flow Method—The Proposal and the Applications," *Bulletin of the Kyushu Institute of Technology* 28 (1974): 33–62.

56. N. D. Bibbo, M. L. Larsen, J. Baumgartner, and V. Arora, "An Improved Rainflow Counting Method for Multiaxial Stress States Using the Minimum Circumscribed Circle Method to Identify Shear Stress Ranges," *International Journal of Fatigue* 163 (2022): 106997.

57. H. J. Gough and H. V. Pollard, "The Strength of Metals Under Combined Alternating Stresses," *Proceedings of the Institution of Mechanical Engineers* 131 (1935): 3–103.

58. I. V. Papadopoulos, "Critical Plane Approaches in High-Cycle Fatigue: On the Definition of the Amplitude and Mean Value of the Shear Stress Acting on the Critical Plane," *Fatigue and Fracture of Engineering Materials and Structures* 21 (1998): 269–285.

59. L. Susmel, "A Simple and Efficient Numerical Algorithm to Determine the Orientation of the Critical Plane in Multiaxial Fatigue Problems," *International Journal of Fatigue* 32 (2010): 1875–1883.

60. N. Z. Faruq and L. Susmel, "Proportional/Nonproportional Constant/Variable Amplitude Multiaxial Notch Fatigue: Cyclic Plasticity, Non-Zero Mean Stresses, and Critical Distance/Plane," *Fatigue and Fracture of Engineering Materials and Structures* 42 (2019): 1849–1873.

61. L. Susmel and D. Taylor, "A Critical Distance/Plane Method to Estimate Finite Life of Notched Components Under Variable Amplitude Uniaxial/Multiaxial Fatigue Loading," *International Journal of Fatigue* 38 (2012): 7–24.

62. E. Niemi, *Stress Determination for Fatigue Analysis of Welded Components* (Cambridge, UK: Woodhead Publishing, 1995).

63. C. M. Sonsino, W. Fricke, F. De Bruyne, A. Hoppe, A. Ahmadi, and G. Zhang, "Notch Stress Concepts for the Fatigue Assessment of Welded Joints—Background and Applications," *International Journal of Fatigue* 34 (2012): 2–16.

64. W. Fricke, "IIW Guideline for the Assessment of Weld Root Fatigue," *Welding in the World* 57 (2013): 753–791.

65. R. Archer, "Fatigue of a Welded Steel Attachment Under Combined Direct Stress and Shear Stress," in *International Conference of Fatigue of Welded Constructions*, vol. 50 (Brighton, UK: The Welding Institute, 1987).

66. M. Bäckström, *Multiaxial Fatigue Life Assessment of Welds Based on Nominal and Hot Spot Stresses* (Espoo, Finland: VTT Technical Research Centre of Finland, 2003).

67. H. Amstutz, K. Störzel, and T. Seeger, "Fatigue Crack Growth of a Welded Tube–Flange Connection Under Bending and Torsional Loading," *Fatigue and Fracture of Engineering Materials and Structures* 24 (2001): 357–368.

68. J. D. M. Costa, L. M. P. Abreu, A. C. M. Pinho, and J. A. M. Ferreira, "Fatigue Behaviour of Tubular AlMgSi Welded Specimens Subjected to Bending–Torsion Loading," *Fatigue and Fracture of Engineering Materials and Structures* 28 (2005): 399–407.

69. J. Wiebesiek andn C. M. Sonsino, "New Results in Multiaxial Fatigue of Welded Aluminium Joints," IIW-Document No XIII-2314-10/XV-1349-10, 13 (2010): 2310–2314.

70. J. Wiebesiek, K. Störzel, T. Bruder, and H. Kaufmann, "Multiaxial Fatigue Behaviour of Laserbeam-Welded Thin Steel and Aluminium Sheets Under Proportional and Non-Proportional Combined Loading," *International Journal of Fatigue* 33 (2011): 992–1005.

71. G. R. Razmjoo, "Fatigue of Load-Carrying Fillet Welded Joints Under Multiaxial Loading," in *5th International Conference on Biaxial/Multiaxial Fatigue & Fracture* (Cambridge, UK: The Welding Institute, 1997): 53–70.

72. E. Shams and M. Vormwald, "Fatigue of Weld Ends Under Combined Loading," *International Journal of Fatigue* 100 (2017): 627–638.

73. C. M. Sonsino. "Fatigue Behaviour of Welded Components Under Complex Elasto-Plastic Multiaxial Deformations," ECSC-Report No EUR 16024 (1997).

74. M. Kueppers and C. M. Sonsino, "Critical Plane Approach for the Assessment of the Fatigue Behaviour of Welded Aluminium Under Multiaxial Loading," *Fatigue and Fracture of Engineering Materials and Structures* 26 (2003): 507–513.

75. M. Kueppers and C. M. Sonsino, "Assessment of the Fatigue Behaviour of Welded Aluminium Joints Under Multiaxial Spectrum Loading by a Critical Plane Approach," *International Journal of Fatigue* 28 (2006): 540–546.

76. C. M. Sonsino, M. Kueppers, M. Eibl, and G. Zhang, "Fatigue Strength of Laser Beam Welded Thin Steel Structures Under Multiaxial Loading," *International Journal of Fatigue* 28 (2006): 657–662.

77. A. Siljander, P. Kurath, and F. V. Lawrence, Jr., *Proportional and Non-Proportional Multiaxial Fatigue of Tube to Plate Weldments* (Urbana, Illinois: University of Illinois Urbana-Champaign, 1989).

78. J.-Y. Yung and F. V. Lawrence, Jr., "Predicting the Fatigue Life of Welds Under Combined Bending and Torsion," in *Biaxial and Multiaxial Fatigue* (London: Mechanical Engineering Publications, 1989): 53–69.

79. F. Yousefi, M. Witt, and H. Zenner, "Fatigue Strength of Welded Joints Under Multiaxial Loading: Experiments and Calculations," *Fatigue and Fracture of Engineering Materials and Structures* 24 (2001): 339–355.

80. B. Pyttel, P. Grawenhof, and C. Berger, "Application of Different Concepts for Fatigue Design of Welded Joints in Rotating Components in Mechanical Engineering," *International Journal of Fatigue* 34 (2012): 35–46.

81. B. Atzori, "Trattamento Termici e Resistenza a Fatica Delle Strutture Soldate," (1983).

82. L. Susmel and R. Tovo, "On the Use of Nominal Stresses to Predict the Fatigue Strength of Welded Joints Under Biaxial Cyclic Loading," *Fatigue and Fracture of Engineering Materials and Structures* 27 (2004): 1005–1024.

83. C. M. Sonsino, "A Consideration of Allowable Equivalent Stresses for Fatigue Design of Welded Joints According to the Notch Stress Concept With the Reference Radii r_{ref} = 1.00 and 0.05 mm," *Welding in the World* 53 (2009): R64–R75.

84. D. Rennert, E. Kullig, M. Vormwald, A. Esderts, and D. Siegele, *Analytical Strength Assessment of Components Made of Steel, Cast Iron and Aluminium Materials in Mechanical Engineering: FKM Guidel*, 6th ed. (Frankfurt/Main, Germany: Forschungskuratorium Maschinenbau (FKM), 2013).

85. E. Haibach, *Fatigue Strength* (Düsseldorf, Germany: VDI-Verlag, 1989).

86. K. Walat and T. Łagoda, "Lifetime of Semi-Ductile Materials Through the Critical Plane Approach," *International Journal of Fatigue* 67 (2014): 73–77.

87. E. John, J. Boxall, R. Collins, E. Bowman, and L. Susmel, "Multiaxial Fatigue of Water Pipe Grey Cast Iron," *International Journal of Fatigue* 178 (2024): 108002.

88. K.-G. Eulitz, "Damage Accumulation Limitations and Perspectives for Fatigue Life Assessment," *Proceedings of Materials Week* 2000 (2000): 25–28.

89. C. M. Sonsino, "Fatigue Testing Under Variable Amplitude Loading," *International Journal of Fatigue* 29 (2007): 1080–1089.

90. D. Radaj, C. M. Sonsino, and W. Fricke, *Fatigue Assessment of Welded Joints by Local Approaches* (Cambridge, UK: Woodhead Publishing, 2006).

91. A. F. Hobbacher, "The New IIW Recommendations for Fatigue Assessment of Welded Joints and Components—A Comprehensive Code Recently Updated," *International Journal of Fatigue* 31 (2009): 50–58.

92. G. Alencar, A. de Jesus, J. G. S. da Silva, and R. Calçada, "A Finite Element Post-Processor for Fatigue Assessment of Welded Structures Based on the Master S-N Curve Method," *International Journal of Fatigue* 153 (2021): 106482.

93. L. Susmel and R. Tovo, "Local and Structural Multiaxial Stress States in Welded Joints Under Fatigue Loading," *International Journal of Fatigue* 28 (2006): 564–575.

94. P. Lazzarin and R. Tovo, "A Notch Intensity Factor Approach to the Stress Analysis of Welds," *Fatigue and Fracture of Engineering Materials and Structures* 21 (1998): 1089–1103.

95. R. Tovo and P. Lazzarin, "Relationships Between Local and Structural Stress in the Evaluation of the Weld Toe Stress Distribution," *International Journal of Fatigue* 21 (1999): 1063–1078.

96. C. Morgenstern, C. M. Sonsino, A. Hobbacher, and F. Sorbo, "Fatigue Design of Aluminium Welded Joints by the Local Stress Concept With the Fictitious Notch Radius of r_f=1 mm," *International Journal of Fatigue* 28 (2006): 881–890.

97. D. Radaj, P. Lazzarin, and F. Berto, "Generalised Neuber Concept of Fictitious Notch Rounding," *International Journal of Fatigue* 51 (2013): 105–115.

98. C. M. Sonsino, T. Bruder, and J. Baumgartner, "SN Lines for Welded Thin Joints—Suggested Slopes and FAT Values for Applying the Notch Stress Concept with Various Reference Radii," *Welding in the World* 54 (2010): R375–R392.

99. L. Susmel, C. M. Sonsino, and R. Tovo, "Accuracy of the Modified Wöhler Curve Method Applied Along With the r_{ref} = 1 mm Concept in Estimating Lifetime of Welded Joints Subjected to Multiaxial Fatigue Loading," *International Journal of Fatigue* 33 (2011): 1075–1091.

100. J. Schijve, "Fatigue Predictions of Welded Joints and the Effective Notch Stress Concept," *International Journal of Fatigue* 45 (2012): 31–38.

101. D. Taylor, "The Theory of Critical Distances," *Engineering Fracture Mechanics* 75 (2008): 1696–1705.

102. L. Susmel, "The Theory of Critical Distances: A Review of Its Applications in Fatigue," *Engineering Fracture Mechanics* 75 (2008): 1706–1724.

103. L. Susmel, "Modified Wöhler Curve Method, Theory of Critical Distances and Eurocode 3: A Novel Engineering Procedure to Predict the Lifetime of Steel Welded Joints Subjected to Both Uniaxial and Multiaxial Fatigue Loading," *International Journal of Fatigue* 30 (2008): 888–907.

104. D. Taylor, N. Barrett, and G. Lucano, "Some New Methods for Predicting Fatigue in Welded Joints," *International Journal of Fatigue* 24 (2002): 509–518.

105. L. Susmel, "Eurocode 3's Standard Curves and Theory of Critical Distances to Estimate Fatigue Lifetime of Steel Weldments," *Key Engineering Materials* 348 (2007): 21–24.

106. P. Lazzarin and P. Livieri, "Notch Stress Intensity Factors and Fatigue Strength of Aluminium and Steel Welded Joints," *International Journal of Fatigue* 23 (2001): 225–232.

107. P. Livieri and P. Lazzarin, "Fatigue Strength of Steel and Aluminium Welded Joints Based on Generalised Stress Intensity Factors and Local Strain Energy Values," *International Journal of Fracture* 133 (2005): 247–276.